

1 Reconstruction of global surface ocean $p\text{CO}_2$ using 2 region-specific predictors based on a stepwise FFNN 3 regression algorithm

4 Guorong Zhong^{1,2,3,4}, Xuegang Li^{1,2,3,4*}, Jinming Song^{1,2,3,4*}, Baoxiao Qu^{1,3,4}, Fan
5 Wang^{1,2,3,4}, Yanjun Wang^{1,4}, Bin Zhang^{1,4}, Xiaoxia Sun^{1,2,3,4}, Wuchang Zhang^{1,3,4},
6 Zhenyan Wang^{1,3,4}, Jun Ma^{1,3,4}, Huamao Yuan^{1,2,3,4}, Liqin Duan^{1,2,3,4}

7 ¹Institute of Oceanology, Chinese Academy of Sciences, Qingdao 266071, China

8 ²University of Chinese Academy of Sciences, Beijing 101407, China

9 ³Pilot National Laboratory for Marine Science and Technology, Qingdao 266237, China

10 ⁴Center for Ocean Mega-Science, Chinese Academy of Sciences, Qingdao 266071,
11 China

12 *Correspondence to:* Xuegang Li (lixuegang@qdio.ac.cn); Jinming Song
13 (jmsong@qdio.ac.cn)

14 **Abstract:** Various machine learning methods were attempted in the global mapping of
15 surface ocean partial pressure of CO_2 ($p\text{CO}_2$) to reduce the uncertainty of global ocean
16 CO_2 sink estimate due to undersampling of $p\text{CO}_2$. In previous researches the predictors
17 of $p\text{CO}_2$ were usually selected empirically based on theoretic drivers of surface ocean
18 $p\text{CO}_2$ and same combination of predictors were applied in all areas unless lack of
19 coverage. However, the differences between the drivers of surface ocean $p\text{CO}_2$ in
20 different regions were not considered. In this work, we combined the stepwise
21 regression algorithm and a Feed Forward Neural Network (FFNN) to selected
22 predictors of $p\text{CO}_2$ based on mean absolute error in each of the 11 biogeochemical
23 provinces defined by Self-Organizing Map (SOM) method. Based on the predictors
24 selected, a monthly global $1^\circ \times 1^\circ$ surface ocean $p\text{CO}_2$ product from January 1992 to
25 August 2019 was constructed. Validation of different combination of predictors based
26 on the SOCAT dataset version 2020 and independent observations from time series
27 stations was carried out. The prediction of $p\text{CO}_2$ based on region-specific predictors
28 selected by the stepwise FFNN algorithm were more precise than that based on
29 predictors from previous researches. Applying of a FFNN size improving algorithm in
30 each province decreased the mean absolute error (MAE) of global estimate to 11.32
31 μatm and the root mean square error (RMSE) to 17.99 μatm . The script file of the
32 stepwise FFNN algorithm and $p\text{CO}_2$ product are distributed through the Institute of
33 Oceanology of the Chinese Academy of Sciences Marine Science Data Center (IOCAS;
34 <http://dx.doi.org/10.12157/iocas.2021.0022>, Zhong et al., 2021).

1 Introduction

As a net sink for atmospheric CO₂, global oceans have been thought to have removed about one third of anthropogenic CO₂ since the beginning of the industrial revolution (Sabine et al., 2004; Friedlingstein et al., 2019). However, ~~great differences existed between previous estimates of sea-air CO₂ flux~~, due to large uncertainty in estimates of surface ocean partial pressure of CO₂ ($p\text{CO}_2$), ~~the long-term average global ocean sea-air CO₂ flux during 2001-2015 estimated based on sea-air $p\text{CO}_2$ difference differ from -1.55 to -1.74 PgC yr⁻¹, and the maximum difference between global sea-air CO₂ flux in individual years reached nearly 0.6 PgC yr⁻¹~~ (Rödenbeck et al., 2014; Iida et al., 2015; Landschützer et al., 2014; Denvil-Sommer et al., 2019; Regnier et al., 2013; Schuster et al., 2013; Wanninkhof et al., 2013; Ishii et al., 2014). ~~The magnitude and direction of the flux is largely set by the air-sea $p\text{CO}_2$ difference. surface ocean $p\text{CO}_2$ is an essential parameter to describe the release and uptake for atmospheric CO₂ by the oceans in the data-based method.~~ Greater $p\text{CO}_2$ of surface water than that of overlying air indicating that CO₂ released from oceans to the air, and absorption of CO₂ by oceans happened when the $p\text{CO}_2$ of surface water was lower than that of air. The ocean in these two scenarios is known as oceanic carbon source and oceanic carbon sink respectively. Sparse and uneven observations of surface ocean $p\text{CO}_2$ in time and space severely limited the understanding of interannual variability of oceanic carbon sink, and researches based on different methods were carried out to break this barrier. In earlier studies, traditional unitary and multiple regression methods between surface ocean $p\text{CO}_2$ and its drivers was attempted in the mapping of surface ocean $p\text{CO}_2$, which were limited in specific regions and sometimes even in specific seasons with a relatively high root mean square error (RMSE) (Sarma et al., 2006; Takahashi et al., 2006; Shadwick et al., 2010; Chen et al., 2011; Marrec et al., 2015). Recent researches on artificial neural networks and other machine learning algorithms, such as feed-forward neural network (FFNN) method (Zeng et al., 2014; Zeng et al., 2015; Moussa et al., 2016; Denvil-Sommer et al., 2019) and self-organization mapping (SOM) method (Friedrich and Oeschies, 2009; Telszewski et al., 2009; Hales et al., 2012; Nakaoka et al., 2013), significantly reduced the bias in the interpolation based on relationships between surface ocean $p\text{CO}_2$ and its drivers. In addition, methods such as finding better predictors or combining SOM and other neural networks ~~was-were~~ also attempt to further decrease the $p\text{CO}_2$ predicting error (Hales et al., 2012; Nakaoka et al., 2013; Landschützer et al., 2014; Chen et al., 2019; Denvil-Sommer et al., 2019; Zhong et al., 2020; Wang et al., 2021). However, the selection of predictors in the surface ocean

70 $p\text{CO}_2$ mapping was more empirical, focusing on the theoretical drivers of the $p\text{CO}_2$ and
71 its variation. Sea surface temperature and salinity, related to the solubility of CO_2 in
72 seawater, were considered as the most important and used in almost all related studies
73 (Landsch~~ü~~etzer et al., 2013; Nakaoka et al., 2013; Moussa et al., 2016; Laruelle et al.,
74 2017; Zeng et al., 2017; Denvil-Sommer et al., 2019), ~~similarly~~ Similarly, the
75 chlorophyll-a concentration is also widely used (Nakaoka et al., 2013; Landsch~~ü~~etzer
76 et al., 2014; Laruelle et al., 2017; Zeng et al., 2017; Denvil-Sommer et al., 2019), which
77 is related to the phytoplankton uptake of CO_2 . One more indicator, mixed layer depth,
78 appeared frequently in related studies as a proxy related to the vertical transport of
79 dissolved carbon (Telszewski et al., 2009; Nakaoka et al., 2013; Landsch~~ü~~etzer et al.,
80 2014; Zeng et al., 2017; Denvil-Sommer et al., 2019). Besides, the sampling
81 information have been also used as indicators, including latitude and longitude
82 (Friedrich and Oeschies, 2009; Jo et al., 2012; Zeng et al., 2015; Zeng et al., 2017;
83 Denvil-Sommer et al., 2019), and sampling time (Friedrich and Oeschies, 2009; Zeng
84 et al., 2015). In recent researches, dry air mixing ratio of atmospheric CO_2 ($x\text{CO}_2$),
85 related to the CO_2 level in air, was also used as a predictor of surface ocean $p\text{CO}_2$
86 (Landsch~~ü~~etzer et al., 2014; Denvil-Sommer et al., 2019). The sea surface height,
87 which was considered effective in improving the spatial pattern and the accuracy of
88 surface ocean $p\text{CO}_2$ mapping at the basin and regional scale, and the monthly anomalies
89 of the most widely used parameters mentioned above were used by the Denvil-Sommer
90 et al (2019). In the research focused on the surface ocean $p\text{CO}_2$ mapping of coastal
91 areas, the bathymetry, sea ice and wind speed were also used as indicators (Laruelle et
92 al., 2017). In each of these researches, same combination of indicators was applied in
93 all areas of the global ocean, although the global ocean was divided into several
94 biogeochemical provinces in some of the researches. However, the indicator that plays
95 an important role in the surface ocean $p\text{CO}_2$ reconstruction at one region may be not a
96 good predictor of surface ocean $p\text{CO}_2$ in other regions, due to complex and variable
97 drivers in different regions. But no widely recognized methods for judging the
98 importance of each predictor in the surface ocean $p\text{CO}_2$ mapping are available yet.
99 Thus, we attempted to construct a stepwise FFNN algorithm to rank the importance of
100 predictors and figure out the optimal combination in each biogeochemical province
101 defined by SOM, for decreasing the predication errors in the surface ocean $p\text{CO}_2$
102 mapping.

103 **2 Methodology**

104 **2.1 Data**

105 The surface ocean fugacity of CO₂ ($f\text{CO}_2$) observation data from the Surface Ocean
 106 CO₂ Atlas $f\text{CO}_2$ dataset version 2020 (SOCATv2020) (Bakker et al., 2016) was used to
 107 construct the non-linear relationship between surface ocean $p\text{CO}_2$ and predictors. The
 108 ~~conversion transition~~ between $f\text{CO}_2$ and $p\text{CO}_2$ was following the formula (Körtzinger,
 109 1999):

$$110 \quad f\text{CO}_2 = p\text{CO}_2 \cdot \exp\left(P \cdot \frac{B+2\delta}{RT}\right) \quad (1)$$

111 where $f\text{CO}_2$ and $p\text{CO}_2$ are in micro-atmospheres (μatm), P is the total atmospheric
 112 surface pressure (Pa) using the National Centers for Environmental Prediction (NCEP)
 113 monthly mean sea level pressure product (Dee et al., 2011), and T is the absolute
 114 temperature (K). R is the gas constant ($8.314 \text{ J K}^{-1} \text{ mol}^{-1}$). Parameters B ($\text{m}^3 \text{ mol}^{-1}$) and
 115 δ ($\text{m}^3 \text{ mol}^{-1}$) are both virial coefficients (Weiss, 1974).

116 In this work, ~~parts of total 33~~ indicators ~~was were~~ used (Table S1). ~~Where 21~~
 117 ~~indicators were chosen~~ from previous researches of surface ocean $p\text{CO}_2$
 118 reconstruction based on machine learning methods, including sea surface temperature
 119 (SST) and sea surface salinity (SSS) using the $1^\circ \times 1^\circ$ gridded product (Cheng et al.,
 120 2016; Cheng et al., 2017; Cheng et al., 2020) ~~from Chen et al (2017)~~ at
 121 ~~http://159.226.119.60/cheng/http://www.ocean.iap.ac.cn/~~ and the anomalies (SST_{anom}
 122 and SSS_{anom}), chlorophyll-a concentration (CHL-a) and the anomaly (CHL-a_{anom}) using
 123 satellite derived monthly product in 9 km resolution (NASA Goddard Space Flight
 124 Center, Ocean Ecology Laboratory, Ocean Biology Processing Group ~~Hu et al.,~~
 125 ~~2012~~2018), mixed layer depth (MLD) and sea surface height (SSH) and the anomalies
 126 (MLD_{anom} and SSH_{anom}) using the ECCO2 cube92 daily product (Menemenlis et al.,
 127 2008), ~~W velocity of ocean currents (W_{vel}) at 5, 65, 105 and 195 m depth using the~~
 128 ~~ECCO2 cube92 3-day product (Menemenlis et al., 2008)~~, dry air mixing ratio of
 129 atmospheric CO₂ ($x\text{CO}_2$) and the anomaly ($x\text{CO}_2$ _{anom}) from the GLOBAL VIEW
 130 marine boundary layer product (GLOBALVIEW-CO2, 2011), sea ice area fraction
 131 using the monthly product from ECMWF ERA Interim (Dee et al., 2011), 10 meters
 132 wind speed using the monthly product from ECMWF ERA Interim (Dee et al., 2011),
 133 bathymetry from ETOPO2 (Commerce et al., 2006) , year and month (represented by
 134 1-12), the total number of months since January 1992 (N_{mon}), the sine of latitude and
 135 the sine and cosine of longitude (sLat, sLon and cLon). In addition, ~~8-12~~ parameters
 136 which were only used in similar previous research focused on other parameters
 137 (Broullón et al., 2019; Broullón et al., 2020), or were possibly related to the driver of
 138 surface ocean $p\text{CO}_2$ and its variability, were selected to be tested. These parameters
 139 included nitrate, phosphate, silicate and dissolved oxygen (DO) using the monthly

140 climatology product from WOA18 (Garcia et al., 2019a, b), sea level pressure (SLP)
141 and surface pressure from the ECMWF ERA Interim (Dee et al., 2011), W velocity of
142 ocean currents (W_{vel}) at 5, 65, 105 and 195 m depth using the ECCO2 cube92 3-day
143 product (Menemenlis et al., 2008), the Oceanic Nino Index (ONI) (Huang et al., 2017),
144 the Southern Hemisphere Annular Mode Index (SAM) (Marshall, G. J., 2003). Most of
145 these products were retrieved at $1^\circ \times 1^\circ$ resolution. Some products retrieved at higher
146 resolution were downscaled to $1^\circ \times 1^\circ$ resolution.

147 **2.2 Biogeochemical provinces defined by the Self-Organizing Map**

148 For applying different combination of indicators in regions based on the differences
149 in the dominated drivers of pCO_2 and its variability, the global ocean was divided into
150 a set of biogeochemical provinces using a Self-Organizing Map (SOM) method. The
151 monthly climatology of temperature, salinity, mixed layer depth, sea surface height,
152 nitrate, phosphate, silicate, and dissolved oxygen and pCO_2 climatology from
153 Landschützer et al, 2020 were put into a 3-by-4 size SOM networks to generate 12
154 biogeochemical provinces, where the monthly climatology data in all 12 months were
155 put into one SOM network to generate one discrete set of biogeochemical provinces.
156 Provinces with connected pixels less than 10 and provinces with SOCAT observation
157 less than 1000 were define as discrete small “island” provinces, and then merged with
158 nearest provinces. Then the discrete small “island” provinces and provinces lack of
159 SOCAT pCO_2 data were merged into the nearest dominated province, and t
160 the provinces covering areas separated by land were further divided artificially. For
161 example, the province covering north subtropical Pacific and the province covering
162 north subtropical Atlantic were set as one province in the original output of SOM, but
163 were mainly separated by The North American continent. So, we divided the province
164 into two new provinces. The final version includes total 11 biogeochemical provinces.
165 In this study the coastal area was not involved and the boundary was defined as 200m
166 depth. In addition, the pCO_2 mapping based on SOM defined provinces tend to be less
167 smooth near the border of different biogeochemical provinces, with obvious border line
168 appearing. However, applying of different predictors may make this problem worse. To
169 obtain a smoother distribution, we defined that the area within 5 1x1 grids of province
170 boundaries as a ‘boundary area’. Samples in the boundary area will be used as training
171 samples in all adjacent provinces (Fig. S1). But this definition does not change the
172 actual spatial coverage of each province, only brings more training samples near the
173 province boundary. ~~extended the boundaries of all provinces 5 $1^\circ \times 1^\circ$ grids width~~
174 outside (Fig. S1). ~~For one sample near the boundary, it is a ‘original sample’ in only one~~

province and is a 'boundary sample' in other provinces. Thus, the sample was involved in the validation of only one province, and was involved in the training process in other provinces as 'boundary sample'. defined that the grid within $5^{\circ} \times 1^{\circ}$ grids of province borders belong to all provinces adjacent to the nearest province border. Samples in these grids were involved in the FFNN training process of multiple provinces, but only counted once in the validation.

2.3 Stepwise FFNN algorithm

For finding better combination of $p\text{CO}_2$ predictors, a stepwise Feed-forward neural networks (FFNN) algorithm was constructed. The FFNN is composed of four main parts, which are namely input, hidden, summation and output layer (Fig. 21). The input layer is designed to pass the inputs to the hidden layer and the number of neurons is equal to the dimensions of the input matrix p . The hidden layer includes 25 neurons in the FFNN model, with the tan-sigmoid function as the transfer function. The input p is multiplied by a matrix of weights (w_1 in Fig. 21) and the inner product between the result and a bias matrix (b_1 in Fig. 21) is calculated as the input of the transfer function in the first hidden layer. In the summation layer, the transfer function f_2 is a pure linear function. The output of the hidden layer is multiplied by another matrix of weights and summed. All bias and weights matrixes were randomly assigned in the beginning of FFNN training. Here we set one constant random number stream in the MATLAB, thus the way that the bias and weights matrixes randomly assigned were steady, avoiding the appearance of inconsistent results when algorithm repeats.

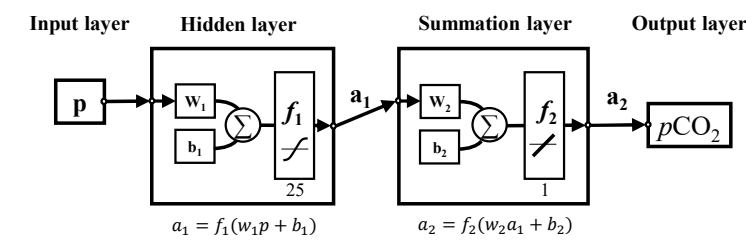
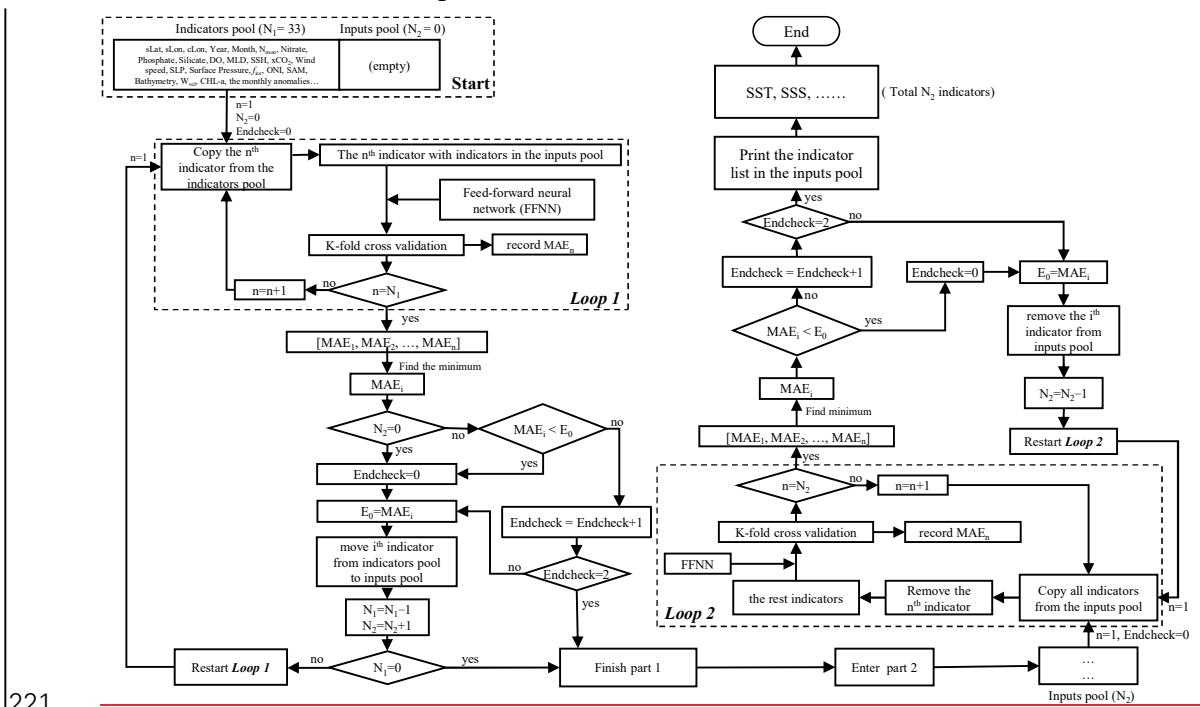


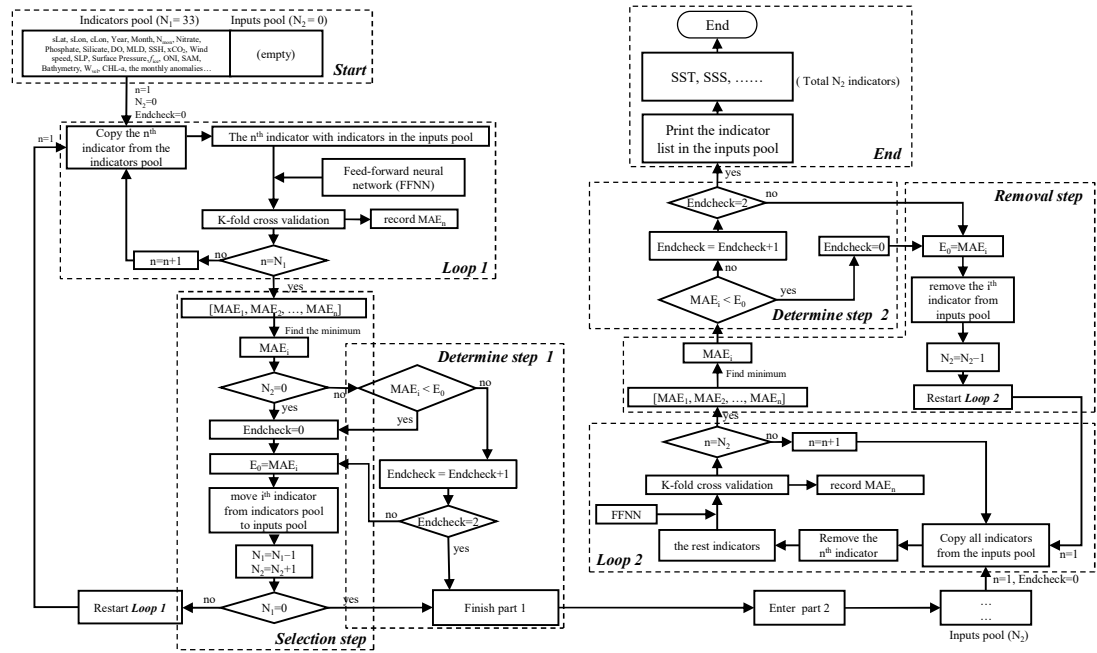
Figure 21. The structure of feed-forward neural network. p : input matrix; w : weighted matrix; b : bias matrix; Σ : sum; f_1 : tan-sigmoid transfer function; f_2 : pure linear function; a : output matrix.

In the stepwise part, predictors of $p\text{CO}_2$ are going to be added and removed one by one, and which predictors will be finally used in the $p\text{CO}_2$ predicting is determined according to the real-time change of predicating error. We used the idea of the multiple linear stepwise regression, replacing the linear regression part by a Feed-forward neural networks (FFNN). The mean absolute error (MAE) difference that before and after

205 adding or removing one indicator in the input of FFNN calculated using a K-fold cross
 206 validation method was used to estimate the performance of each indicator in the FFNN
 207 predicating. Although the root mean square error (RMSE) was widely used for the
 208 validation of machine learning methods. Compared to the MAE, the RMSE was more
 209 sensitive to a few extreme samples, which were generally deviated far from the FFNN
 210 predicting values, resulting in a huge discrepancy between the FFNN outputs and $p\text{CO}_2$
 211 observations sometimes up to hundreds of μatm . A higher weight may be put on these
 212 few extreme samples than other samples in the predictor selection if the performance
 213 of each indicator was estimated by RMSE in the stepwise FFNN algorithm. To avoid
 214 the higher weight on these few extreme samples, the MAE was used instead for internal
 215 performance loss function in the stepwise FFNN algorithm. The basic principle of the
 216 stepwise FFNN algorithm was adding each indicator from a set of indicators into the
 217 inputs of FFNN and removing each redundant indicator from the inputs successively to
 218 reduce the MAE between the FFNN outputs and SOCAT $p\text{CO}_2$ values in the fastest way,
 219 until no decrease in the MAE appearing (Fig. 12), where the indicator having no
 220 contribution to reduce the prediction error was considered as redundant.



221



222
 223 Figure 12. ~~the~~The procedure of stepwise FFNN algorithm. The flow-chart is following an order of
 224 “left top – left bottom – right bottom – right top”. The meaning of Indicators pool: store all indicators
 225 waiting to be tested; Inputs pool: store indicators that was temporally considered as good predictors;
 226 Loop 1 and Loop 2: calculate the MAE when each indicator was added as predictors or removed;
 227 Selection step: add good predictors to the Inputs pool; Removal step: remove predictors from the
 228 Inputs pool if removing lead to MAE decrease; Determine step: check if the process reach end
 229 condition. N_1 and N_2 : number of indicators in the Indicators pool and Inputs pool respectively; E_0 :
 230 lowest MAE in the last iteration of Loop 1 or Loop 2; Endcheck: the number of iterations that E_0
 231 continuously increased.

232 In the beginning of the stepwise FFNN algorithm, all available indicators were put
 233 into a matrix, referred to as indicators pool (Start in Fig. 2), where each of rows
 234 represents one indicator and each of columns represents one SOCAT sample. In this
 235 work we collected 33 parameters for test, that is, the indicators pool matrix has 33 rows.
 236 Meanwhile a matrix, referred to as inputs pool (Start in Fig. 2), was set up to storage
 237 indicators with good performance, where good performance means that adding these
 238 indicators as predictors can significantly decrease the MAE between SOCAT pCO_2
 239 measurements and FFNN pCO_2 predictions. Then a loop of K-fold validation test run
 240 out to calculate the MAE that predicting pCO_2 by each one indicator in the indicators
 241 pool in the first step (Loop-Loop 1 in the Fig. 12). Thus total 33 MAE values were
 242 obtained and the minimum was recorded as E_0 . The indicator that corresponds to the
 243 minimum of all MAE values was moved from the indicators pool to the inputs pool
 244 (Selection step in the Fig. 2). After that the loop 1 restarted, i.e., the second step started

245 with one indicator removed to the inputs pool and the rest 32 indicators waiting to be
246 tested. Then 32 MAE values of predicting $p\text{CO}_2$ by each one of the rest indicators in
247 the indicators pool with the addition of all indicators in the inputs pool were calculated
248 out. If the MAE in the lowest situation, represented by the MAE_i , decreased compared
249 to the E_0 , the i^{th} indicator was considered as a good indicator and was moved from the
250 indicators pool to the inputs pool as well. Then the value of E_0 was replaced by the
251 MAE_i (*Selection step in the Fig. 2*). ~~This~~ *The part 1, including loop 1, Selection step*
252 *and Determine step in the Fig. 2*, was repeated that the good indicators were selected
253 out in one-by-one step and moved to the inputs pool in the way that the E_0 decreases in
254 the fastest way, until no indicator was left in the indicators pool or no decrease can be
255 found no matter which indicator was added in the next two steps (*Determine step 1 in*
256 *the Fig. 2*). At this time the part 1 of stepwise FFNN algorithm finished, and all
257 indicators left in the indicators pool were considered redundant. The loop K-fold
258 validation in the second part run out in a opposite way that the MAE was calculated
259 with the indicators were removed from the inputs pool one by one in the way that the
260 E_0 decreases the fastest (~~loop~~ *Loop 2* in Fig. 42). The second part was aimed to remove
261 the indicator that can be represented by other indicators in the inputs pool (*Removal*
262 *step in the Fig. 2*), and finished in the similar condition that no significant decrease can
263 be found no matter which indicator was removed in the next two steps (*Determine step*
264 *2 in the Fig. 2*).

265 ~~The FFNN is composed of four main parts, which are namely input, hidden,~~
266 ~~summation and output layer (Fig.2). The input layer is designed to pass the inputs to~~
267 ~~the hidden layer and the number of neurons is equal to the dimensions of the input~~
268 ~~matrix p . The hidden layer includes 25 neurons in the FFNN model, with the tan-~~
269 ~~sigmoid function as the transfer function. The input p is multiplied by a matrix of~~
270 ~~weights (w_1 in Fig. 2) and the inner product between the result and a bias matrix (b_1 in~~
271 ~~Fig. 2) is calculated as the input of the transfer function in the first hidden layer. In the~~
272 ~~summation layer, the transfer function f_2 is a pure linear function. The output of the~~
273 ~~hidden layer is multiplied by another matrix of weights and summed. All bias and~~
274 ~~weights matrixes were randomly assigned in the beginning of FFNN training. Here we~~
275 ~~set one constant random number stream in the MATLAB, thus the way that the bias and~~
276 ~~weights matrixes randomly assigned were steady, avoiding the appearance of~~
277 ~~inconsistent results when algorithm repeats.~~

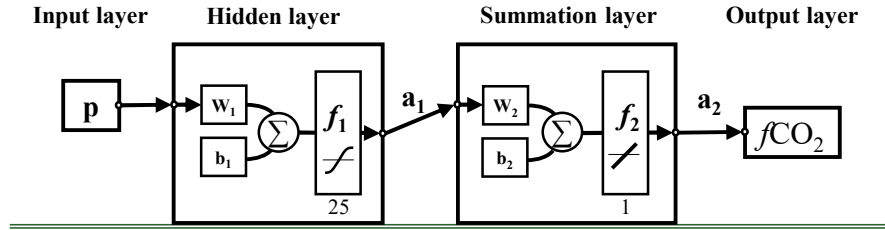


Figure 2. The structure of feed-forward neural network. p : input matrix; w : weighted matrix; b : bias matrix; Σ : sum; f_1 : tan-sigmoid transfer function; f_2 : pure linear function; a : output matrix.

2.4 $p\text{CO}_2$ product

Dataset of parameters except CHL-a start since 1992 or earlier, while CHL-a data ranges from August 2002 to present. In each one of the provinces, the stepwise FFNN algorithm was run out once first based on all samples covered by CHL-a data, then the algorithm was run out secondly based on samples and all indicators except CHL-a and CHL-a_{anom} in the year that CHL-a gridded data was not available. The $p\text{CO}_2$ mapping in the year that CHL-a gridded data was not available was carried out based on the predictors selected in the second run. Then the final product was built based on two FFNNs, one trained for the period from August 2002 to August 2019 using one predictor set including CHL-a or CHL-a_{anom}, and the second one for the period from January 1992 to July 2002 using the second predictor set without CHL-a and CHL-a_{anom}. Although the performance may improve with the number of neurons increasing, the influence of number of neurons on the performance of FFNN $p\text{CO}_2$ prediction remains unclear. To further decrease the predicating error between FFNN outputs and SOCAT measurements, the number of neurons was improved by an error test in each province. The number of neurons increased from 10-5 to 70-300 and the corresponding MAE values of each size were record, and then the number of neurons with lowest MAE was applied. This test avoided the appearance of insufficient learning capacity for complex nonlinear relationship due to too few neurons and overfitting problem due to too many neurons. Finally, based on the indicators selected by the stepwise FFNN algorithm and improved FFNN size, a monthly global $1^\circ \times 1^\circ$ surface ocean $p\text{CO}_2$ product from January 1992 to August 2019 was constructed.

2.5 Validation

To better estimate the predicating error of FFNN, the MAE and additionally the RMSE which was widely used in previous researches, were calculated using a K-fold cross validation method. To avoid overfitting caused by a lack of independence between the training samples and testing samples, the SOCAT samples were put in chronological order and then divided into group of years (Table 1) (Gregor et al., 2019). In this paper, the value of K was set as 4. Thus, among every 4 neighboring years, three group samples

310 were used for training FFNN model and the rest one was used for testing. Total 4
 311 iterations were carried out, where testing year changed in each iteration. After 4
 312 iterations finished, all samples have been used for testing only once, and the MAE and
 313 RMSE between FFNN output and the testing samples was calculated. The performance
 314 of the predictor selection algorithm was estimated by comparing the MAE and RMSE
 315 result of the FFNN based on stepwise selected indicators with the result based on
 316 indicators used in previous researches in each biogeochemical province (Table 2). All
 317 validation groups were applied with same FFNN and same samples from SOCAT, with
 318 the only differences in predictors. Same K-fold validation procedure was applied for
 319 three validation groups based on different $p\text{CO}_2$ predictors. Thus, three results were
 320 generated to estimate whether the stepwise FFNN algorithm can effectively find better
 321 combination of $p\text{CO}_2$ predictors. Finally the $p\text{CO}_2$ data generated in all validation
 322 groups were further compared with the completely independent observations from the
 323 Hawaii Ocean Time-series (HOT, 22° 45'N, 158° 00'W, since October 1988) (Dore et
 324 al., 2009), Bermuda Atlantic Time-series Study (BATS, 31°50'N, 64°10'W, since
 325 October 1988) (Bates, 2007) and The European Station for Time Series in the Ocean
 326 Canary Islands (ESTOC, 29°10'N, 15°30'W, from 1995 to 2009) (González-Dávila and
 327 Santana-Casiano, 2009) time series station. These observations were not included in the
 328 SOCAT dataset.

329 Table 1. The procedure of K-fold validation.

	FFNN training	FFNN testing															
1 st iteration	1992	1993	1994	1995	1996	1997	1998	1999	...	2012	2013	2014	2015	2016	2017	2018	2019
2 nd	1992	1993	1994	1995	1996	1997	1998	1999	...	2012	2013	2014	2015	2016	2017	2018	2019
3 rd	1992	1993	1994	1995	1996	1997	1998	1999	...	2012	2013	2014	2015	2016	2017	2018	2019
4 th iteration	1992	1993	1994	1995	1996	1997	1998	1999	...	2012	2013	2014	2015	2016	2017	2018	2019

330
 331 (The K value was set as 4, so iterations repeated four times until all samples have been set as testing
 332 samples once. In each iteration, samples in 7 years were set as testing samples (green cells) and in
 333 the rest 21 years as training samples (white cells) to increase the independency.)

334 Table 2. validation-Validation group using different predictors

Validation group	Predictor
FFNN1	Indicators selected by stepwise FFNN algorithm
FFNN2	SST, SSS, $\log_{10}(\text{MLD})$, CHL-a, $x\text{CO}_2$, SST_{anom} , SSS_{anom} , $x\text{CO}_2_{\text{anom}}$, CHL-a anom , $\log_{10}(\text{MLD})_{\text{anom}}$ (Landschüetter et al., 2014)

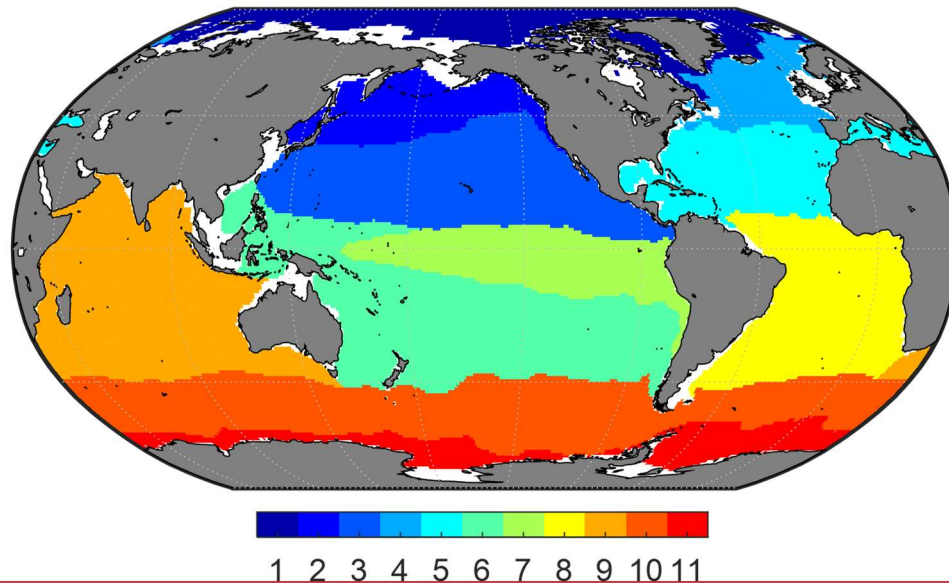
FFNN3 SST, SSS, SSH, MLD, xCO₂, CHL-a, SSS_{anom}, SST_{anom}, SSH_{anom}, CHL-a_{anom},
MLD_{anom}, xCO_{2anom}, sLat, sLon, cLon (Denvil-Sommer et al., 2019)

335 [\(The FFNN performance of three groups with different predictors of \$p\text{CO}_2\$ were compared, to test](#)
336 [the result of stepwise FFNN algorithm. Predictors in the group FFNN1 were selected using stepwise](#)
337 [FFNN algorithm, and predictors in the group FFNN2 were selected from Landschützer et al. \(2014\),](#)
338 [and in the group FFNN3 from Denvil-Sommer et al. \(2019\).\)](#)

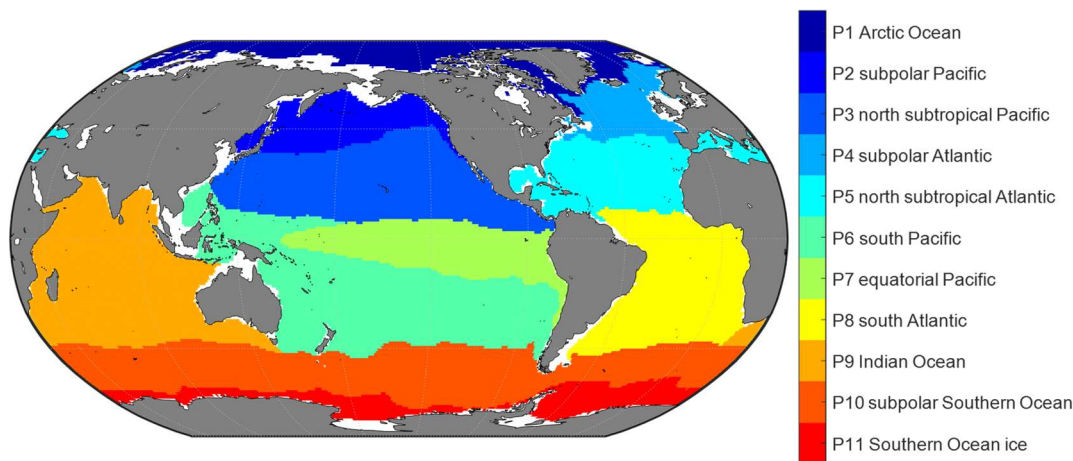
339 **3 Results and discussion**

340 **3.1 Biogeochemical provinces and corresponding predictors of $p\text{CO}_2$**

341 11 biogeochemical provinces generated from the SOM method after the separated
342 small ‘island’ was removed and the province separated by lands was divided manually
343 (Fig. 3). The results of the stepwise FFNN algorithm in each province were shown in
344 the Table 3. The indicators were listed in the order that the stepwise FFNN algorithm
345 printed recommended predictors out. The indicator printed earlier was relatively more
346 recommended and played an important role in the prediction of $p\text{CO}_2$ based on FFNN.
347 Applying of these indicators as the predictors of surface ocean $p\text{CO}_2$ effectively
348 decreased the predicating error between the FFNN outputs and $p\text{CO}_2$ values from
349 validation samples, thus it is reasonable to consider that these indicators were highly
350 related to the drivers of $p\text{CO}_2$ and its variability. Indicators representing sampling
351 position were also listed as recommended predictors in some provinces, including
352 latitude, longitude and sampling time, suggesting that relatively steady spatial or
353 temporal variability pattern of surface ocean $p\text{CO}_2$ existed in these biogeochemical
354 provinces. For example, month was considered as a recommended predictor in most
355 provinces. Especially in the provinces ~~covering the north Atlantic Ocean~~ (P4 [subpolar](#)
356 [Atlantic](#) and P5 [north subtropical Atlantic](#)), the parameter month was relatively more
357 recommended. While $p\text{CO}_2$ in these areas regularly peaked and bottomed out in
358 summer and winter (Takahashi et al., 2009; Landschützer et al., 2016; Landschützer
359 et al., 2020). Similarly, latitude and the sine and cosine of longitude were listed as
360 recommended predictors of $p\text{CO}_2$ in most provinces, suggesting an obvious spatial
361 distribution pattern of $p\text{CO}_2$, which was not learned sufficiently by the FFNN model
362 from existing indicators and the indicators related to spatial position were applied as
363 supplementary.



364



365

366 Figure 3. The map of biogeochemical provinces

366

367

368

369

370

371

372

373

374

375

376

377

378

379

As basic parameters highly related to the ocean environment, the temperature and salinity was considered as parts of the most important predictors of surface ocean $p\text{CO}_2$, and was applied in the $p\text{CO}_2$ prediction in almost all previous relating researches based on various method (Jo et al., 2012; Signorini et al., 2013; Landschüetzer et al., 2014; Marrec et al., 2015; Chen et al., 2016; Moussa et al., 2016; Chen et al., 2017; Laruelle et al., 2017; Zeng et al., 2017; Chen et al., 2019; Denvil-Sommer et al., 2019). The results of stepwise FFNN algorithm also supported this. Temperature was listed as a recommended predictor in all biogeochemical provinces, suggesting that temperature was the one of the most important drivers of $p\text{CO}_2$ and its variability in these provinces. Similarly, the result of stepwise FFNN algorithm ~~provides evidence for~~proved the importance of salinity in the predication of $p\text{CO}_2$, which was also listed as a predictor in most provinces. ~~In the province P1 located in the Arctic, the silicate concentration and temperature were considered as the most crucial predictor of $p\text{CO}_2$.~~ The dry air

380 mixing ratio of atmospheric CO₂ (xCO₂) and the monthly anomaly of xCO₂ were also
381 recommended predictors in most of the biogeochemical provinces, suggesting that the
382 exchange of CO₂ across the sea-air interface was also an important driver of surface
383 ocean pCO₂. As a widely used predictor in the pCO₂ prediction, the chlorophyll-a
384 concentration (CHL-a) played an important role in fitting the influence of biological
385 activities on pCO₂ in previous researches (Landschuetzer et al., 2014; Zeng et al., 2017;
386 Laruelle et al., 2017; Denvil-Sommer et al., 2019). Especially in the province P10
387 subpolar Southern Ocean (~~province P10~~ and P11) Southern Ocean ice, the CHL-a was
388 listed as the most recommended predictor in the result of stepwise FFNN algorithm.
389 While in some other provinces (P1 Arctic Ocean and P5 north subtropical Atlantic), the
390 CHL-a were considered redundant that no effective decrease of MAE between FFNN
391 outputs and pCO₂ measurements appeared when CHL-a data was used. Similar with the
392 period that CHL-a was not available (represented by the subscript ‘b’), the phosphate,
393 nitrate, silicate or dissolved oxygen were recommended instead. In the province P1
394 Arctic Ocean, the silicate concentration and temperature were considered as the most
395 crucial predictor of pCO₂.

396 Table 3. Predictors in each biogeochemical province

Province	Predictors <u>on the order selected by the stepwise FFNN algorithm</u>
P1 <u>Arctic Ocean</u>	Silicate, SST, Wind speed, SSS, log ₁₀ (MLD), SSS _{anom} , sLat, month, W _{vel} (65m), log ₁₀ (MLD) _{anom} , xCO ₂ , cLon, Bathymetry, SSH
P2 <u>subpolar Pacific</u> ^{a*}	Nitrate, CHL-a, SSS, xCO ₂ , cLon, SST, log ₁₀ (MLD), sLon, sLat, month
P2 <u>subpolar Pacific</u> ^{b*}	Nitrate, xCO _{2anom} , sLon, SST, sLat, log ₁₀ (MLD), cLon, SSS, SSH _{anom} , DO, W _{vel} (195m), Bathymetry, Silicate
P3 <u>north subtropical Pacific</u> ^a	log ₁₀ (MLD), N _{mon} , SSH, SST, sLon, sLat, SSS, Bathymetry, month, log ₁₀ (MLD) _{anom} , cLon, Surface pressure, W _{vel} (105m), CHL-a, DO, SSH _{anom} , xCO _{2anom}
P3 <u>north subtropical Pacific</u> ^b	log ₁₀ (MLD), xCO ₂ , sLat, sLon, SST, Surface pressure, cLon, SSS, W _{vel} (5m), N _{mon} , log ₁₀ (MLD) _{anom} , month, Phosphate, xCO _{2anom} , W _{vel} (105m)
P4 <u>subpolar Atlantic</u> ^a	month, sLat, cLon, SST, Year, CHL-a, DO, SSS _{anom} , W _{vel} (195m), SSH, log ₁₀ (MLD), Bathymetry, SSS
P4 <u>subpolar Atlantic</u> ^b	month, xCO ₂ , DO, Wind speed, log ₁₀ (MLD), W _{vel} (195m), sLon, Bathymetry, W _{vel} (5m), SST, Phosphate, Year, N _{mon}
P5 <u>north subtropical Atlantic</u>	month, Year, SST, sLon, sLat, SSS, SST _{anom} , SSH, Bathymetry, W _{vel} (5m), cLon, W _{vel} (65m), log ₁₀ (MLD) _{anom}
P6 <u>south Pacific</u> ^a	SST, sLon, xCO _{2anom} , sLat, SSS, month, Phosphate, CHL-a, CHL-a _{anom} ,

	W _{vel} (65m), log ₁₀ (MLD), log ₁₀ (MLD) _{anom} , Nitrate, Bathymetry
P6 <u>south Pacific</u> _b	xCO ₂ , sLat, SSS, SST, Phosphate, SLP, xCO ₂ _{anom} , sLon, cLon, W _{vel} (105m), W _{vel} (65m), DO, Bathymetry, SSH, SAM
P7 _a <u>equatorial Pacific</u>	Nitrate, xCO ₂ , sLat, SSS, SST, cLon, xCO ₂ _{anom} , log ₁₀ (MLD), sLon, CHL-a, Phosphate, W _{vel} (5m), W _{vel} (105m), W _{vel} (195m)
P7 _b <u>equatorial Pacific</u>	SST, SSS, Year, sLat, month, cLon, SSH, Bathymetry, W _{vel} (65m), xCO ₂
P8 <u>south Atlantic</u> _a	sLat, xCO ₂ _{anom} , SSS, log ₁₀ (MLD), CHL-a, SSH _{anom} , W _{vel} (195m), cLon, SST, W _{vel} (65m), Bathymetry, Nitrate
P8 <u>south Atlantic</u> _b	SST, xCO ₂ , cLon, sLat, SSS, Silicate, SSH, log ₁₀ (MLD), sLon
P9 <u>Indian Ocean</u> _a	SST, cLon, sLat, Nitrate, W _{vel} (65m), log ₁₀ (MLD), SLP, CHL-a, Year, log ₁₀ (MLD) _{anom} , SSH _{anom}
P9 <u>Indian Ocean</u> _b	SLP, month, sLon, xCO ₂ _{anom} , SST, Silicate, W _{vel} (65m)
P10 <u>subpolar Southern Ocean</u> _a	CHL-a, log ₁₀ (MLD), N _{mon} , SSS, SST, Bathymetry, SSH _{anom} , W _{vel} (5m), CHL- a _{anom} , xCO ₂
P10 <u>subpolar Southern Ocean</u> _b	Wind speed, xCO ₂ _{anom} , SSS, Phosphate, log ₁₀ (MLD), W _{vel} (65m), Bathymetry, SST, month
P11 <u>Southern Ocean ice</u> _a	CHL-a, sLon, Bathymetry, SSS, SSH, SST, Nitrate, cLon, sLat
P11 <u>Southern Ocean ice</u> _b	month, DO, SST, SSH, sLat, Nitrate, sLon, SSS, W _{vel} (195m), Silicate, SSH _{anom}

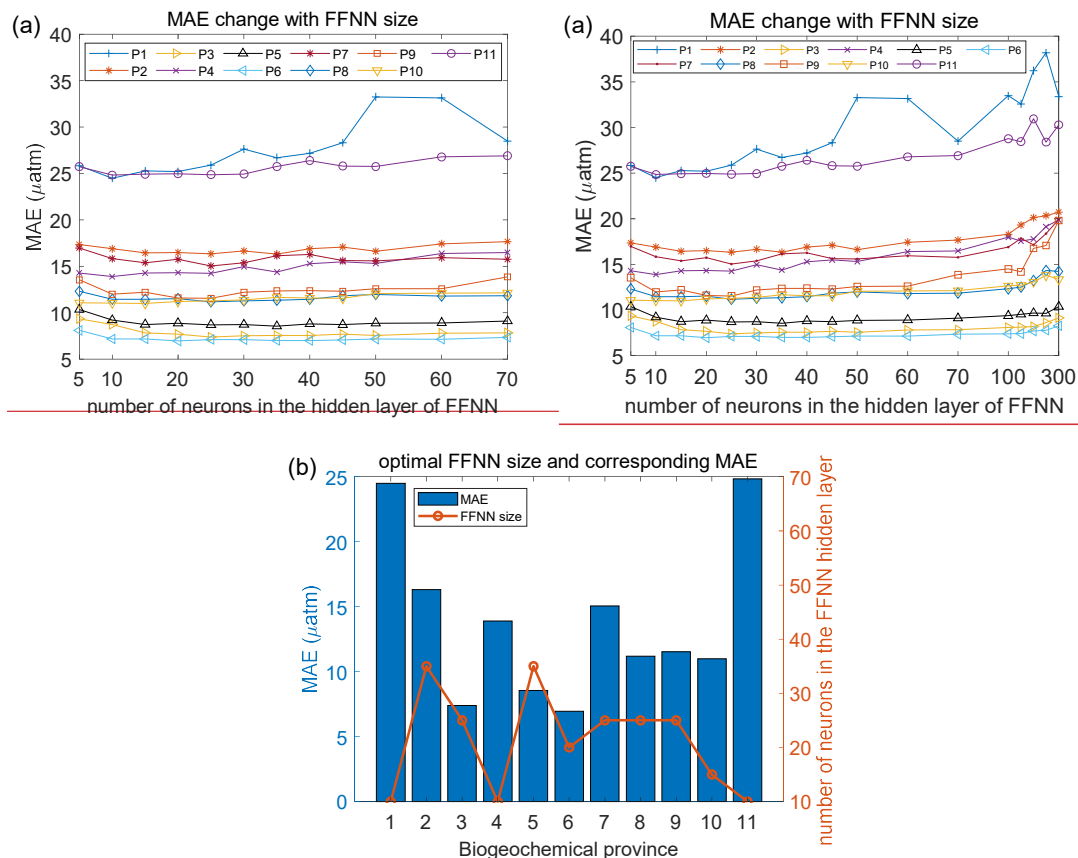
*: Due to insufficient coverage of CHL-a data in the polar areas and during the period before 2002. ~~The pCO₂ data in~~ the province that CHL-a or CHL-a_{anom} ~~was were~~ selected as predictors, ~~the pCO₂ data~~ was divided into two periods. The period that CHL-a data available was represented by the subscript 'a', such as P2_a, including global grids from 2002 to 2019 except polar grids in winter. The period that CHL-a data not available was represented by the subscript 'b', such as P2_b, including global grids from 1992 to 2001 and additionally some polar grids in winter from 1992 to 2019.

397 3.2 pCO₂ product

398 Based on the predictors given by the stepwise FFNN algorithm in each
399 biogeochemical province, a FFNN size (representing the number of neurons in the
400 hidden layer) improving validation was applied to further decrease the predication error.
401 The MAE values based on same samples and FFNN model with different number of
402 neurons were calculated, then the number of neurons corresponding to the lowest MAE
403 were applied (Fig. 4a). The MAE in most provinces tend to decrease first and then
404 increase when the number of neurons in the hidden layer of FFNN model increased
405 from ~~105~~ to ~~70300~~. Based on the variation of MAE with the number of neurons in the
406 FFNN hidden layer, the optimal FFNN size in each province was considered as the
407 number of neurons when the MAE was lowest. The result and corresponding MAE

408 were shown in Fig. 4b. The MAE and RMSE of global estimates between predicted
 409 $p\text{CO}_2$ and measurements from SOCAT v2020 further decreased to 11.32 and 17.99 μatm
 410 respectively after applying optimal FFNN size in each province.

411



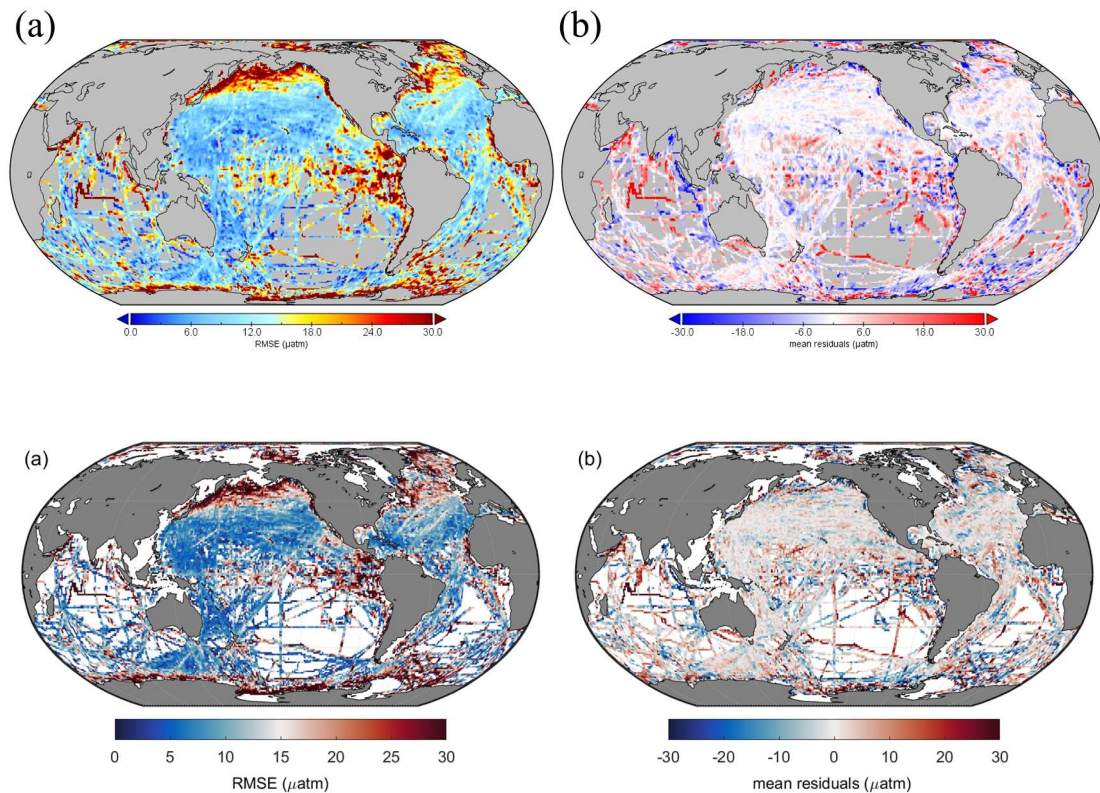
412

413

414 Figure 4. MAE of different FFNN size in each biogeochemical province. a): MAE between
 415 predicted $p\text{CO}_2$ and SOCAT observations were calculated using same samples and FFNN with
 416 different number of neurons. b): the optimal FFNN size was referring to the number of neurons
 417 when MAE is lowest.

418

419 Then the RMSE and mean residuals in each grid were calculated based on the K-
 420 fold cross validation method. In most grids, the RMSE was lower than 10 μatm and the
 421 mean residuals was close to zero (Fig. 5). However, the prediction error in the north
 422 subpolar Pacific, the east equatorial Pacific and the Southern Ocean near the Antarctic
 423 continent was obviously higher than other areas. Also, dDistribution of mean residuals
 424 suggested that surface ocean $p\text{CO}_2$ in the Indian Ocean tend to be overestimated by the
 425 FFNN models. While in other regions the distribution of mean residuals was more
 discrete and no obvious pattern was found.

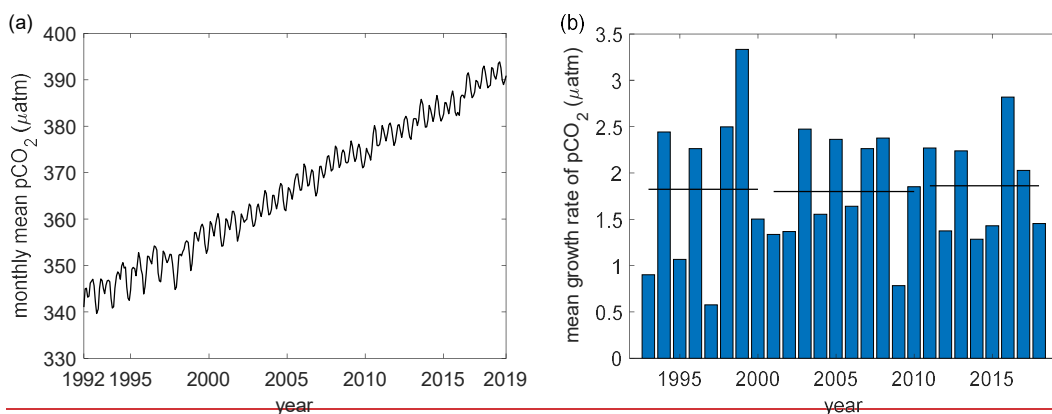


426

427

428 Figure 5. Global maps of (a) RMSE and (b) mean residuals between predicted $p\text{CO}_2$ and SOCAT
 429 observations

430 ~~Based on stepwise FFNN algorithm and improved FFNN size in each province, a~~
 431 ~~monthly $1^\circ \times 1^\circ$ grided surface ocean $p\text{CO}_2$ product from January 1992 to August 2019~~
 432 ~~was constructed. The interannual variability of global average $p\text{CO}_2$ was showed in the~~
 433 ~~Fig. 6. The global open-ocean average $p\text{CO}_2$ increased about $1.85 \mu\text{atm}$ per year from~~
 434 ~~1992 to 2019.~~



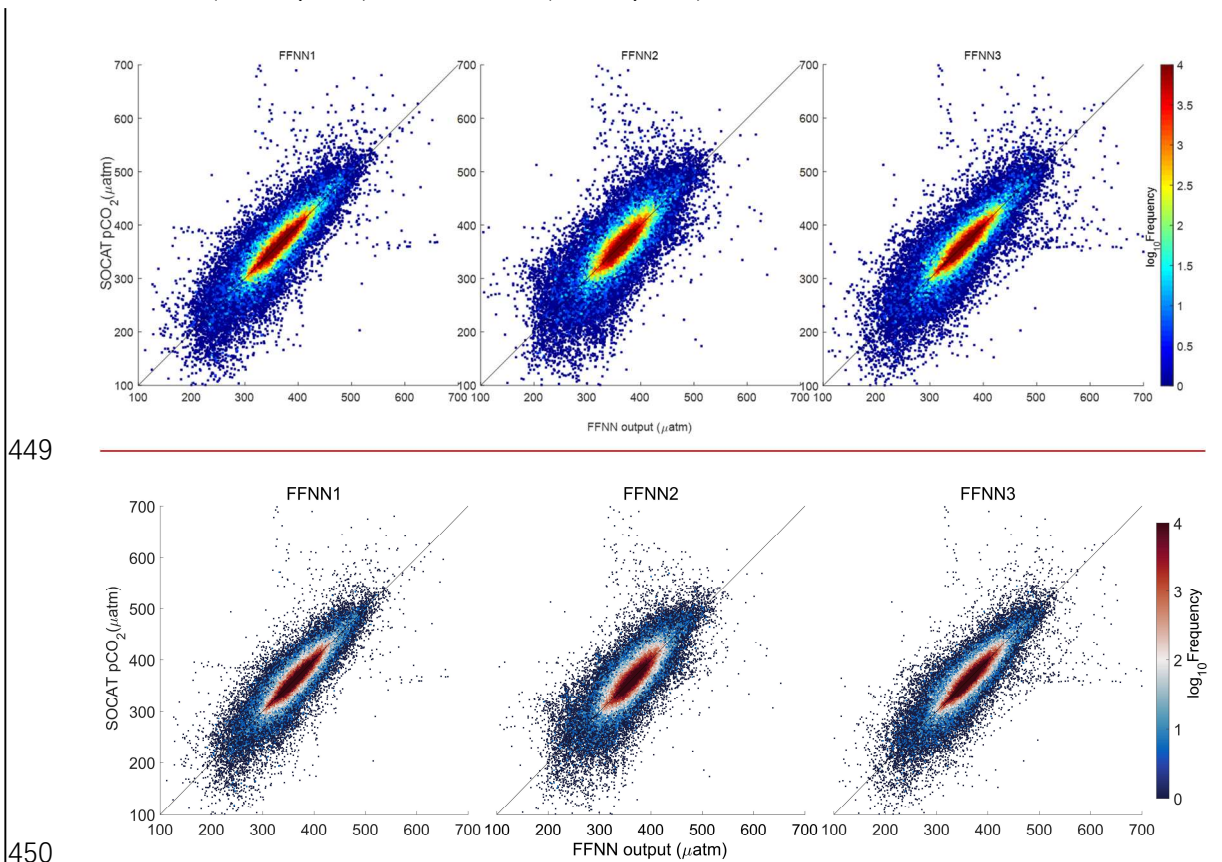
435

436 Figure 6. Interannual variability of global open-oceanic $p\text{CO}_2$ during 1992-2019. (a): global
 437 monthly mean $p\text{CO}_2$, (b): growth rate of global monthly mean $p\text{CO}_2$

438 3.3 Validation of the stepwise FFNN algorithm based on SOCAT samples

439 Validation based on the K-fold cross validation method suggested that most FFNN

440 outputs were quite close to the $p\text{CO}_2$ values from SOCAT v2020 samples (Fig. 76).
 441 Comparing the results based on different combination of predictors, the results of
 442 FFNN1 (based on stepwise FFNN algorithm, this paper) and FFNN3 (based on 15
 443 predictors from Denvil-Sommer, et al. 2019) were **obviously** more precise than that of
 444 FFNN2 (based on 10 predictors from Landschüetter, et al. 2014). Where the plots in
 445 the result of FFNN1 was most concentrated along the $y=x$ line, suggesting extremely
 446 close FFNN outputs with the measured $p\text{CO}_2$ values from SOCAT, with the RMSE of
 447 17.99 μatm in the global open oceans. The RMSE of FFNN1 was lower than that of
 448 FFNN2 (22.95 μatm) and FFNN3 (19.17 μatm).



449
 450
 451 Figure 76. Comparing of FFNN predicted $p\text{CO}_2$ with SOCAT $p\text{CO}_2$. FFNN1 was based on
 452 predictors selected by the stepwise-FFNN algorithm. FFNN2 and FFNN3 were based on predictors
 453 from Landschüetter et al., 2014 and Denvil-Sommer et al., 2019 respectively.

454 For specific comparison of accuracy in each province, the MAE of FFNN1 was
 455 lower in most provinces (Table. 4), except the relatively close results between the
 456 FFNN1 and FFNN3 in parts of provinces. Where the MAE of FFNN1 in the province
 457 P9 **Indian Ocean** was significantly lower than that of the other validation groups,
 458 suggesting a better combination of predictors highly related to the drivers of surface
 459 ocean $p\text{CO}_2$ and its variability in the Indian Ocean. Compared with predictors of

460 FFNN2 and FFNN3, the predictors of FFNN1 added surface pressure and W velocity
461 of ocean currents, and abandoned the monthly anomalies of other indicators in the
462 province P9 Indian Ocean. The low relevance between pCO₂ and part of the monthly
463 anomalies, such as SSS_{anom} and ~~SSH_{anom}~~SST_{anom}, may be responsible for significant
464 lower MAE of FFNN1. Adding redundant indicators may cause misleading in the
465 learning of FFNN model on the contrary. The MAE and RMSE difference between
466 FFNN1 and FFNN3 in some provinces were relatively small. The reason for higher
467 MAE and RMSE showed by the FFNN2 may be the application of latitudes and
468 longitudes as predictors in both the FFNN1 and FFNN3 but not in the FFNN2. In the
469 province P10 subpolar Southern Ocean, latitudes and longitudes were considered not
470 good predictors by the stepwise FFNN algorithm and the results of three validation
471 groups were extremely close because predictors used in both FFNN1 and FFNN3 were
472 related to main drivers of pCO₂, such as CHL-a, xCO₂ and MLD.

473 Table 4. Performance of the pCO₂ prediction based on different predictors

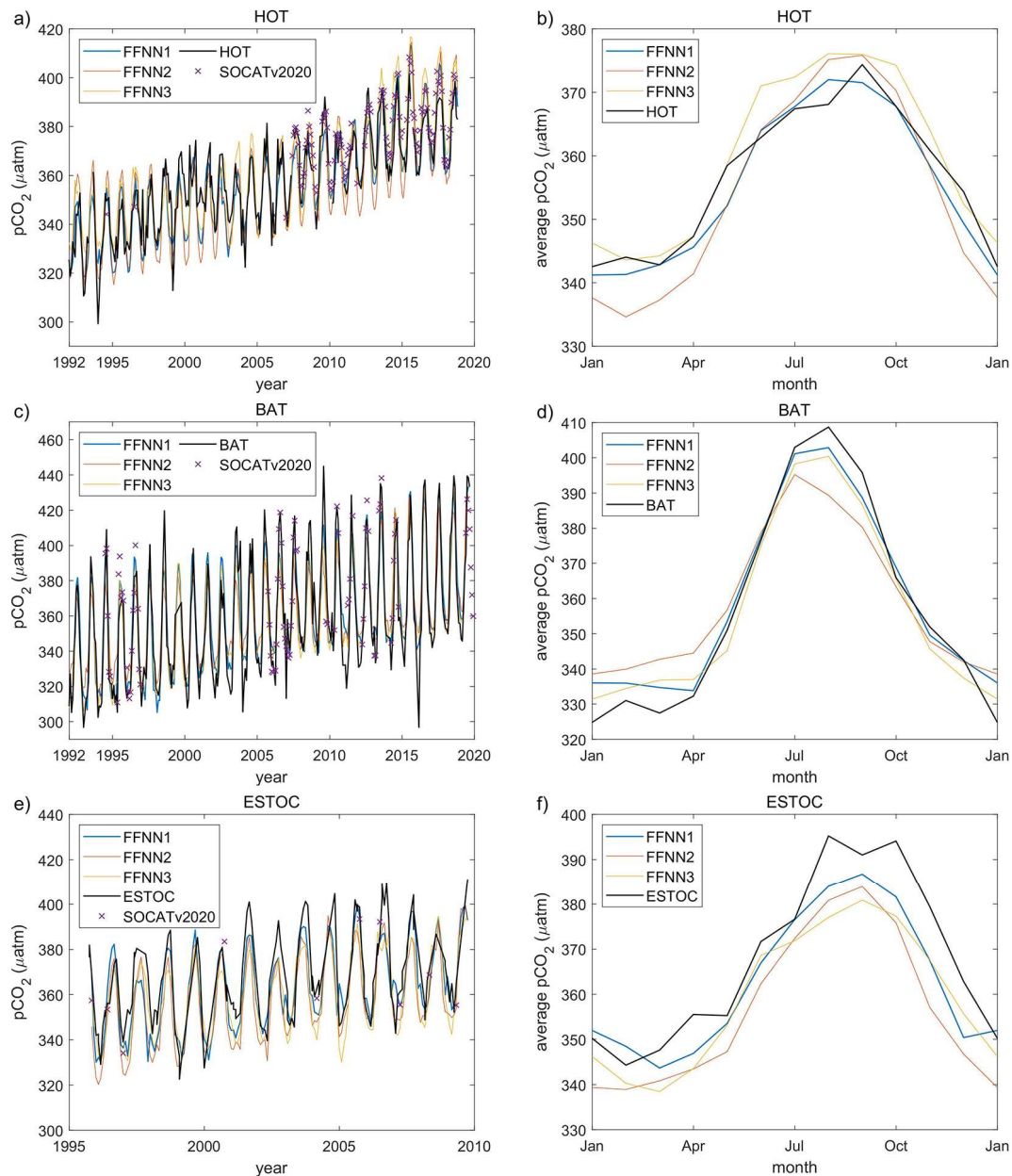
Province	FFNN size	MAE (µatm)			RMSE (µatm)		
		FFNN1	FFNN2	FFNN3	FFNN1	FFNN2	FFNN3
P1 <u>Arctic Ocean</u> (9856)	10	24.50	32.32	26.87	32.27	43.68	35.08
P2 <u>subpolar Pacific</u> (30516)	35	16.32	20.63	16.67	24.32	29.87	25.03
P3 <u>north subtropical Pacific</u> (56367)	25	7.39	12.16	7.95	11.33	17.75	11.88
P4 <u>subpolar Atlantic</u> (29595)	10	13.89	16.91	14.73	21.06	24.29	22.27
P5 <u>north subtropical Atlantic</u> (45358)	35	8.55	12.28	9.00	12.80	17.86	13.72
P6 <u>south Pacific</u> (31803)	20	6.96	9.94	7.24	9.86	14.64	11.00
P7 <u>equatorial Pacific</u> (11233)	25	15.05	19.55	15.49	20.98	27.61	21.10
P8 <u>south Pacific</u> (10259)	25	11.19	15.07	12.43	17.10	20.87	17.66
P9 <u>Indian Ocean</u> (7440)	25	11.54	13.78	15.49	17.15	22.89	28.29
P10 <u>subpolar Southern Ocean</u> (21206)	15	11.00	11.76	12.14	16.61	17.22	17.66
P11 <u>Southern Ocean ice</u> (10683)	10	24.84	29.26	25.74	34.73	40.42	35.22
Global (264316)		11.32	15.08	12.06	17.99	22.95	19.17

474 (FFNN1 was based on predictors selected by the stepwise-FFNN algorithm. FFNN2 and FFNN3
475 were based on predictors from Landschüetter et al., 2014 and Denvil-Sommer et al., 2019
476 respectively.)

477

478 3.4 Validation based on independent observations

479 The FFNN outputs based on different combination of predictors were compared
480 with independent observations from the Ocean Time-series (HOT) (Dore et al., 2009),
481 Bermuda Atlantic Time-series Study (BATS) (Bates, 2007) and The European Station
482 for Time Series in the Ocean Canary Islands (ESTOC) (González-Dávila and Santana-
483 Casiano, 2009) (Fig. 87). ~~The interannual variability and seasonal pattern of $p\text{CO}_2$ in~~
484 ~~the grids the HOT station located from different validation groups were similar and~~
485 ~~close to the observations from the HOT, which was located in the province P3.~~
486 Compared with the independent observations from the HOT station, the three validation
487 groups both show close results, which were also similar with each other in the seasonal
488 and interannual variability of $p\text{CO}_2$. From 1992 to 2019, the RMSE between FFNN1
489 outputs and HOT observations was only 9.29 μatm , lower than the 10.85 μatm of
490 FFNN2 and the 10.70 μatm of FFNN3. The monthly mean $p\text{CO}_2$ of FFNN2 during
491 winter was ~~obviously~~ lower than the HOT observations and $p\text{CO}_2$ values of other
492 validation groups, while the FFNN1 and FFNN3 outputs were closer to the HOT
493 observations. MAE between predicted $p\text{CO}_2$ and HOT observations were also lower in
494 the validation group FFNN1, which was only 7.17 μatm , compared to the 8.61 μatm of
495 FFNN2 and the 8.44 μatm of FFNN3. Higher bias generated in the winter bottom and
496 summer peak, which was showed more obviously in the monthly average of $p\text{CO}_2$ (Fig.
497 8b7b). Compared with other validation groups, the result of FFNN1 was closer to the
498 monthly average values of the HOT observations. Same conclusion can be obtained in
499 the ESTOC and BATS station located in the province P5 north subtropical Atlantic. The
500 RMSE between FFNN1 outputs and independent observations were 13.03 μatm in the
501 BATS station and 11.35 μatm in the ESTOC station, lower than that of other validation
502 groups. The RMSE between FFNN2 outputs and independent observations was 16.15
503 μatm in the BATS station and 14.51 μatm in the ESTOC station. For the group FFNN3,
504 the RMSE was 13.09 μatm in the BATS station and 13.01 μatm in the ESTOC station.
505 All results were extremely close to the independent observations, but the RMSE and
506 MAE of FFNN1 were lower. Similar with the situation in the HOT station, the FFNN1
507 was most close and the FFNN3 second. Based on the better performance of FFNN1, in
508 which the predictors selected by stepwise FFNN algorithm were used, we may
509 conclude that the stepwise FFNN algorithm can effectively find better combination of
510 predictors to fit the diver of surface ocean $p\text{CO}_2$ and obtained lower error.



511

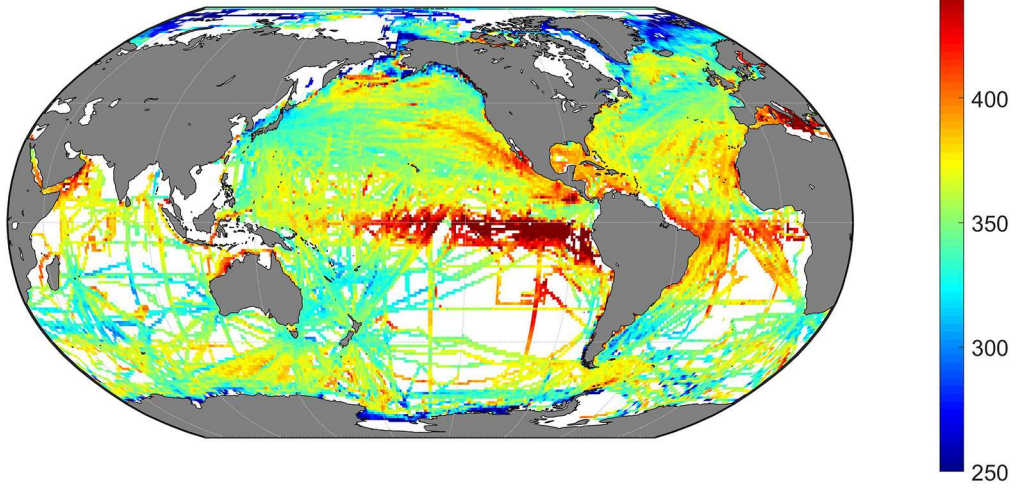
512 Figure 87. Validation based on independent observation from time series stations. a) and b): the
 513 Hawaii Ocean Time-series (HOT) (Dore et al., 2009); c) and d): the Bermuda Atlantic Time-series
 514 Study (BATS) (Bates, 2007); e) and f): the European Station for Time Series in the Ocean Canary
 515 Islands (ESTOC) (González-Dávila and Santana-Casiano, 2009) time series station. FFNN1 was
 516 based on predictors selected by the stepwise-FFNN algorithm. FFNN2 and FFNN3 were based on
 517 predictors from Landschützer et al., 2014 and Denvil-Sommer et al., 2019 respectively.
 518 SOCATv2020 represents the monthly mean $p\text{CO}_2$ of SOCAT observations in the corresponding
 519 grids of each time series station.

520 3.5 Climatological spatial distribution

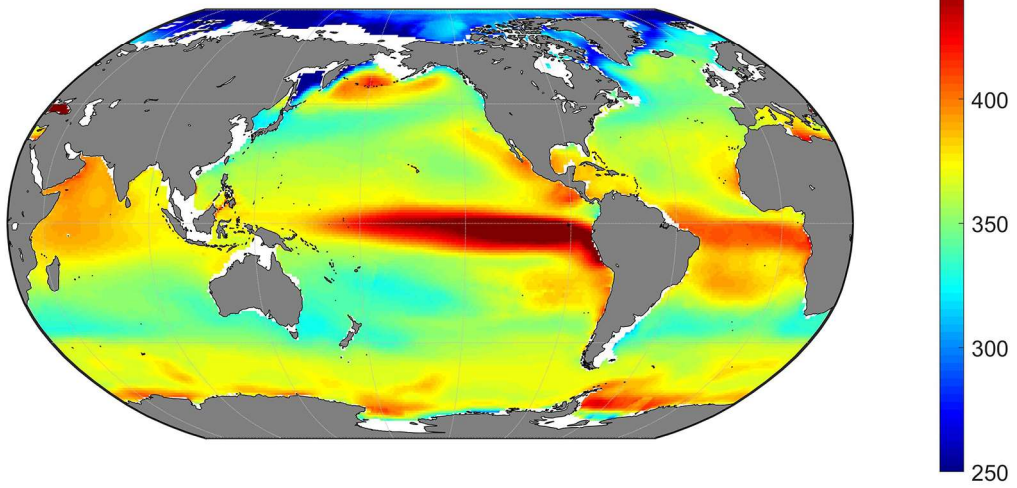
521 The climatological average distribution of $p\text{CO}_2$ suggested a significant spatial
 522 variability (Fig. 98), which is consistent with the average distribution of SOCAT

523 observations. In the Pacific Ocean, the high $p\text{CO}_2$ areas showed by the stepwise-FFNN
524 product (Fig. 9b8b), including the equatorial areas, east temperate areas and north
525 subpolar areas, were highly consistent with the SOCAT datasets (Fig. 9a8a). Similarly,
526 the distribution of $p\text{CO}_2$ in the Atlantic Ocean ~~and the Indian Ocean~~ was also close.
527 However, the stepwise-FFNN product suggested lower $p\text{CO}_2$ average values in the
528 Arctic and higher values in the Southern Ocean near the Antarctic continent. Compared
529 with previous climatology product (Landschützer et al., 2020), the stepwise FFNN
530 product have similar spatial patterns with high $p\text{CO}_2$ in the eastern equatorial Pacific
531 and equatorial Atlantic: inconsistent spatial distribution also existed in the Arctic and
532 parts of the Southern Ocean near the Antarctic continent. Compared with previous
533 climatology product (Landschützer et al., 2020), the global distribution pattern of
534 surface ocean $p\text{CO}_2$ was basically well consistent. Inconsistent spatial distribution also
535 existed in the Arctic and parts of the Southern Ocean near the Antarctic continent. The
536 differences between stepwise-FFNN product and previous climatology product may be
537 caused by differences in methods or SOCAT dataset versions used. While lower average
538 values of the SOCAT dataset in the Southern Ocean may be caused by the
539 undersampling in winter. The global spatial distribution pattern of the stepwise FFNN
540 $p\text{CO}_2$ product was basically well consistent with previous climatology product and
541 SOCAT dataset, suggesting that $p\text{CO}_2$ predicting based on regional different predictors
542 selected by the stepwise FFNN algorithm was ~~credible~~ better than that based on the
543 globally same predictors.

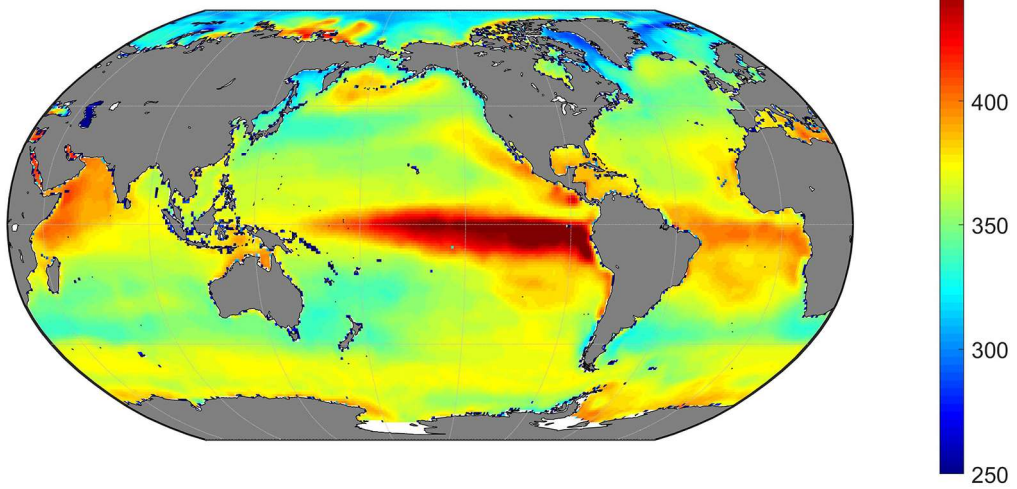
(a) SOCAT v2020 average

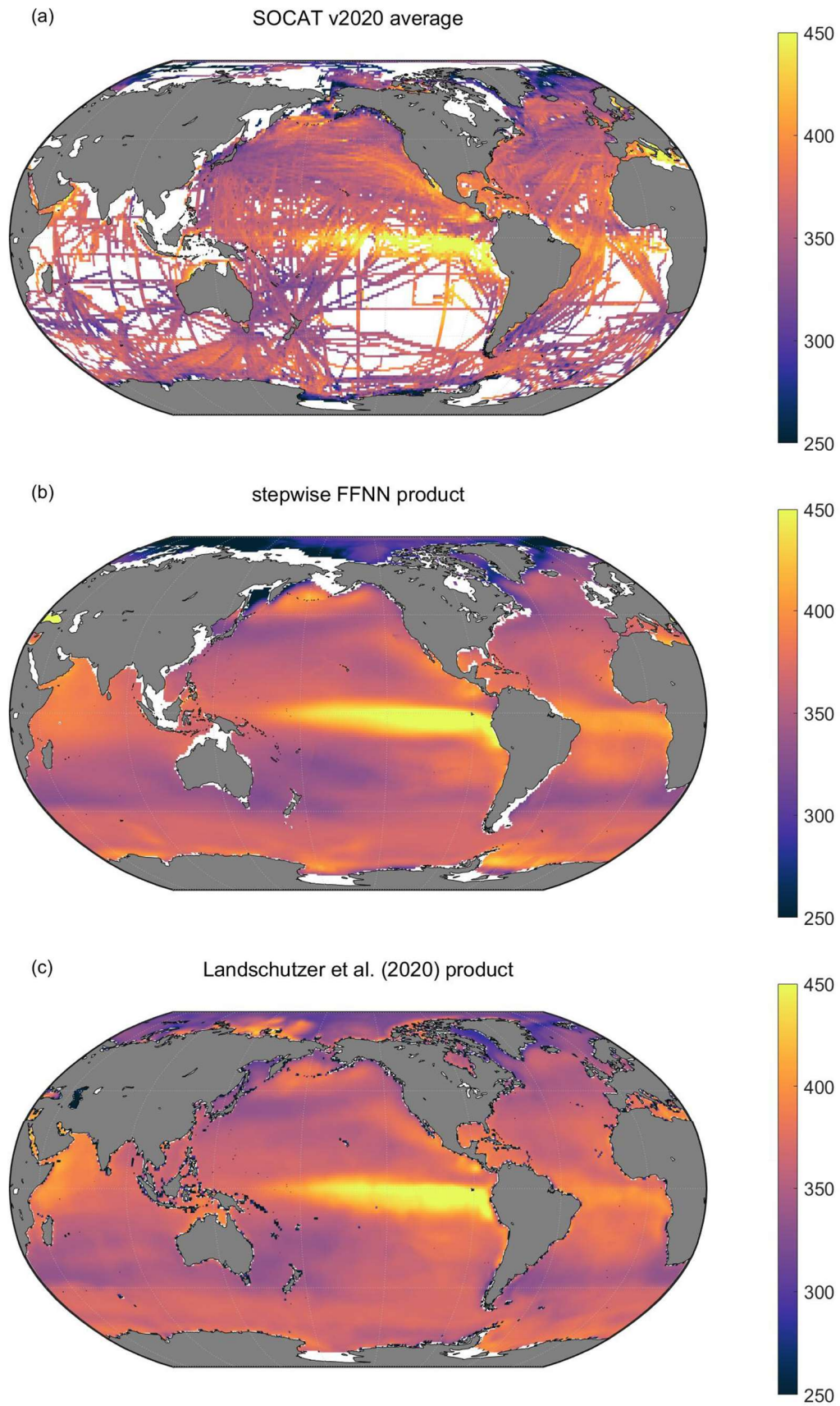


(b) stepwise FFNN product



(c) previous climatology product





545

546

Figure 98. Comparison between long term average of a): SOCAT v2020 dataset, b): the stepwise

547 FFNN $p\text{CO}_2$ product and c): previous climatology product adapted from Landschützer et al., 2020.

548 4. Conclusions

549 A stepwise FFNN algorithm was constructed to decreasing the predicating error in
550 the surface ocean $p\text{CO}_2$ mapping by finding better combinations of $p\text{CO}_2$ predictors in
551 each biogeochemical province defined by SOM method, based on which. ~~Comparing~~
552 ~~with the performance of FFNN based on predictors same with previous researches, the~~
553 ~~RMSE decreased when using predictors selected by the stepwise FFNN algorithm in~~
554 ~~all provinces, suggesting that the stepwise FFNN algorithm was capable to find better~~
555 ~~combination of predictors. In addition, validation based on independent observations~~
556 ~~from HOT, BATS and ESTOC time series stations also proved the better performance~~
557 ~~of FFNN based on predictors selected by the stepwise FFNN algorithm. We further~~
558 ~~decreased the MAE and RMSE of global estimates to 11.32 and 17.99 μatm by~~
559 ~~improving the number of neurons in the hidden layer of FFNN. Then a monthly $1^\circ \times 1^\circ$~~
560 ~~gridded global open-oceanic surface ocean $p\text{CO}_2$ product from January 1992 to August~~
561 ~~2019 was constructed, based improved FFNN size and the predictors selected by~~
562 ~~stepwise FFNN algorithm. Our work provided a statistical way of predictor selection~~
563 ~~for all researches based on relationship fitting by machine learning methods, and shows~~
564 ~~that using regional-specific predictors selected by the stepwise FFNN algorithm~~
565 ~~retrieved lower predicting error than using globally same predictors. This stepwise~~
566 ~~FFNN algorithm can be also used in $p\text{CO}_2$ mapping researches for higher resolution~~
567 ~~and coastal regions, and also in other data mapping researches using SOM or other~~
568 ~~region dividing method. The prepare work was only collecting as many parameters,~~
569 ~~which are possibly related to the target data and need to be sufficiently available in time~~
570 ~~and space. However, high predicting error in special regions still remains to be~~
571 ~~improved, such as polar regions and equatorial Pacific. Since the result of the stepwise~~
572 ~~FFNN largely depends on the way biogeochemical provinces divided, improving of~~
573 ~~SOM step is still necessary. Besides, the FFNN can be replaced by any suitable type of~~
574 ~~neural networks. A possible way to improve the performance of stepwise FFNN~~
575 ~~algorithm is to modify the structure of FFNN or to use better networks. In this study,~~
576 ~~regional specific combination of predictors was first applied in the global surface~~
577 ~~ocean $p\text{CO}_2$ mapping. The result of the stepwise FFNN algorithm was also capable for~~
578 ~~analyzes of driving based on the ranking of relative importance of each predictor. The~~
579 ~~more important predictor, which played a more important role in decreasing the~~
580 ~~predicting error, will be selected earlier and listed at the front of the recommended~~
581 ~~predictor list. In the future work, the stepwise FFNN algorithm with possible~~

582 [improvement](#) will be attempted in the mapping of other parameters, such as total
583 alkalinity and pH, to provide more sufficient data support for studies on ocean
584 acidification and carbon cycling.

585 **Code and data availability**

586 The stepwise FFNN algorithm (as a .m file for MATLAB) and the global $1^{\circ}\times 1^{\circ}$
587 gridded surface ocean $p\text{CO}_2$ product since from January 1992 to August 2019 (as a
588 NetCDF file) generated during this study is available from the Institute of Oceanology
589 of the Chinese Academy of Sciences Marine Science Data Center at
590 <http://dx.doi.org/10.12157/iocas.2021.0022> or directly at
591 <http://english.casodc.com/data/metadata-special-detail?id=1418424272359075841>.

592 **Author contribution**

593 Ma Jun, Yuan Huamao and Duan Liqin collected the dataset of $p\text{CO}_2$ predictors,
594 and Qu baoxiao and Wang Yanjun was contributed in the synthesis of datasets. Zhong
595 Guorong, Li Xuegang and Song Jinming designed the predictor selection algorithm
596 and performed the reconstruction of $p\text{CO}_2$ product. Wang Fan, Zhang Bin, Sun Xiaoxia,
597 Zhang Wuchang, and Wang Zhenyan were contributed in the further improving. Zhong
598 Guorong prepared the manuscript with contributions from all co-authors.

599 **Competing interests**

600 The authors declare that they have no conflict of interest.

601 **Acknowledgement**

602 This work was supported by The National Key Research and Development
603 Program of China (No. 2017YFA0603204), the Strategic Priority Research Program of
604 the Chinese Academy of Sciences (No. XDA19060401), National Natural Science
605 Foundation of China (No. 91958103 and No. 42176200), and Natural Science
606 Foundation of Shandong Province (ZR2020YQ28). We thank SOCAT for sharing the
607 $f\text{CO}_2$ observation data. The Surface Ocean CO_2 Atlas (SOCAT) is an international effort,
608 endorsed by the International Ocean Carbon Coordination Project (IOCCP), the Surface
609 Ocean Lower Atmosphere Study (SOLAS) and the Integrated Marine Biosphere
610 Research (IMBeR) program, to deliver a uniformly quality-controlled surface ocean
611 CO_2 database. The many researchers and funding agencies responsible for the collection
612 of data and quality control are thanked for their contributions to SOCAT. [We thank
613 NASA Goddard Space Flight Center, Ocean Ecology Laboratory, Ocean Biology
614 Processing Group for sharing the Chlorophyll concentration data.](#)

616 **References**

617 Bakker, D. C. E., Pfeil, B., Landa, C. S., Metzl, N., O'Brien, K. M., Olsen, A., Smith,
618 K., Cosca, C., Harasawa, S., Jones, S. D., Nakaoka, S.-i., Nojiri, Y., Schuster, U.,
619 Steinhoff, T., Sweeney, C., Takahashi, T., Tilbrook, B., Wada, C., Wanninkhof, R.,
620 Alin, S. R., Balestrini, C. F., Barbero, L., Bates, N. R., Bianchi, A. A., Bonou, F.,

621 Boutin, J., Bozec, Y., Burger, E. F., Cai, W.-J., Castle, R. D., Chen, L., Chierici, M.,
622 Currie, K., Evans, W., Featherstone, C., Feely, R. A., Fransson, A., Goyet, C.,
623 Greenwood, N., Gregor, L., Hankin, S., Hardman-Mountford, N. J., Harlay, J., Hauck,
624 J., Hoppema, M., Humphreys, M. P., Hunt, C., Huss, B., Ibanhez, J. S. P.,
625 Johannessen, T., Keeling, R., Kitidis, V., Koertzing, A., Kozyr, A., Krasakopoulou,
626 E., Kuwata, A., Landschuetzer, P., Lauvset, S. K., Lefevre, N., Lo Monaco, C.,
627 Manke, A., Mathis, J. T., Merlivat, L., Millero, F. J., Monteiro, P. M. S., Munro, D.
628 R., Murata, A., Newberger, T., Omar, A. M., Ono, T., Paterson, K., Pearce, D., Pierrot,
629 D., Robbins, L. L., Saito, S., Salisbury, J., Schlitzer, R., Schneider, B., Schweitzer,
630 R., Sieger, R., Skjelvan, I., Sullivan, K. F., Sutherland, S. C., Sutton, A. J., Tadokoro,
631 K., Telszewski, M., Tuma, M., van Heuven, S. M. A. C., Vandemark, D., Ward, B.,
632 Watson, A. J., and Xu, S.: A multi-decade record of high-quality $f\text{CO}_2$ data in version
633 3 of the Surface Ocean CO_2 Atlas (SOCAT), *Earth System Science Data*, 8, 383-413,
634 10.5194/essd-8-383-2016, 2016.

635 Bates, N. R.: Interannual variability of the oceanic CO_2 sink in the subtropical gyre of
636 the North Atlantic Ocean over the last 2 decades, *Journal of Geophysical Research:*
637 *Oceans*, 112, 2007.

638 [Broullón, D., Pérez, F. F., Velo, A., Hoppema, M., Olsen, A., Takahashi, T., Key, R. M.,
639 Tanhua, T., González-Dávila, M., Jeansson, E., Kozyr, A., and van Heuven, S. M. A.
640 C.: A global monthly climatology of total alkalinity: a neural network approach,
641 *Earth System Science Data*, 11, 1109-1127, 10.5194/essd-11-1109-2019, 2019.](#)

642 [Broullón, D., Pérez, F. F., Velo, A., Hoppema, M., Olsen, A., Takahashi, T., Key, R. M.,
643 Tanhua, T., Magdalena Santana-Casiano, J., and Kozyr, A.: A global monthly
644 climatology of oceanic total dissolved inorganic carbon: a neural network approach,
645 *Earth System Science Data*, 12, 1725-1743, 10.5194/essd-12-1725-2020, 2020.](#)

646 Chen, L. Q., Xu, S. Q., Gao, Z. Y., Chen, H. Y., Zhang, Y. H., Zhan, J. Q., and Li, W.:
647 Estimation of monthly air-sea CO_2 flux in the southern Atlantic and Indian Ocean
648 using in-situ and remotely sensed data, *Remote Sensing of Environment*, 115, 1935-
649 1941, 10.1016/j.rse.2011.03.016, 2011.

650 [Cheng L. and J. Zhu: Benefits of CMIP5 multimodel ensemble in reconstructing
651 historical ocean subsurface temperature variation, *Journal of Climate*, 29\(15\), 5393–
652 5416, 10.1175/JCLI-D-15-0730.1, 2016.](#)

653 [Cheng L., K. Trenberth, J. Fasullo, T. Boyer, J. Abraham, J. Zhu: Improved estimates
654 of ocean heat content from 1960 to 2015, *Science Advances*, 3, e1601545, 2017.](#)

655 [Cheng L., K. E. Trenberth, N. Gruber, J. P. Abraham, J. Fasullo, G. Li, M. E. Mann, X.
656 Zhao, Jiang Zhu: Improved estimates of changes in upper ocean salinity and the
657 hydrological cycle. *Journal of Climate*, 33, 10357–10381, 10.1175/JCLI-D-20-
658 0366.1, 2020.](#)

659 Chen, S., Hu, C., Barnes, B. B., Wanninkhof, R., Cai, W.-J., Barbero, L., and Pierrot,
660 D.: A machine learning approach to estimate surface ocean $p\text{CO}_2$ from satellite
661 measurements, *Remote Sensing of Environment*, 228, 203-226,
662 10.1016/j.rse.2019.04.019, 2019.

663 Chen, S. L., Hu, C. M., Byrne, R. H., Robbins, L. L., and Yang, B.: Remote estimation
664 of surface $p\text{CO}_2$ on the West Florida Shelf, *Continental Shelf Research*, 128, 10-25,
665 10.1016/j.csr.2016.09.004, 2016.

666 Chen, S. L., Hu, C. M., Cai, W. J., and Yang, B.: Estimating surface $p\text{CO}_2$ in the northern
667 Gulf of Mexico: Which remote sensing model to use?, *Continental Shelf Research*,
668 151, 94-110, 10.1016/j.csr.2017.10.013, 2017.

669 Commerce, U. D. o., Administration, N. O. a. A., and Center, N. G. D.: 2-minute
670 Gridded Global Relief Data (ETOPO2v2).
671 <http://www.ngdc.noaa.gov/mgg/fliers/06mgg01.html>, 2006.

672 Dee, D. P., Uppala, S. M., Simmons, A. J., Berrisford, P., Poli, P., Kobayashi, S., Andrae,
673 U., Balmaseda, M. A., Balsamo, G., Bauer, P., Bechtold, P., Beljaars, A. C. M., van
674 de Berg, L., Bidlot, J., Bormann, N., Delsol, C., Dragani, R., Fuentes, M., Geer, A.
675 J., Haimberger, L., Healy, S. B., Hersbach, H., Holm, E. V., Isaksen, L., Kallberg, P.,
676 Kohler, M., Matricardi, M., McNally, A. P., Monge-Sanz, B. M., Morcrette, J. J., Park,
677 B. K., Peubey, C., de Rosnay, P., Tavolato, C., Thepaut, J. N., and Vitart, F.: The
678 ERA-Interim reanalysis: configuration and performance of the data assimilation
679 system, *Q J Roy Meteor Soc*, 137, 553-597, 10.1002/qj.828, 2011.

680 Denvil-Sommer, A., Gehlen, M., Vrac, M., and Mejia, C.: LSCE-FFNN-v1: a two-step
681 neural network model for the reconstruction of surface ocean $p\text{CO}_2$ over the global
682 ocean, *Geoscientific Model Development*, 12, 2091-2105, 10.5194/gmd-12-2091-
683 2019, 2019.

684 Dore, J. E., Lukas, R., Sadler, D. W., Church, M. J., and Karl, D. M.: Physical and
685 biogeochemical modulation of ocean acidification in the central North Pacific,
686 *Proceedings of the National Academy of Sciences*, 106, 12235-12240, 2009.

687 Friedlingstein, P., Jones, M. W., O'Sullivan, M., Andrew, R. M., Hauck, J., Peters, G. P.,
688 Peters, W., Pongratz, J., Sitch, S., Le Quere, C., Bakker, D. C. E., Canadell, J. G.,
689 Ciais, P., Jackson, R. B., Anthoni, P., Barbero, L., Bastos, A., Bastrikov, V., Becker,
690 M., Bopp, L., Buitenhuis, E., Chandra, N., Chevallier, F., Chini, L. P., Currie, K. I.,
691 Feely, R. A., Gehlen, M., Gilfillan, D., Gkritzalis, T., Goll, D. S., Gruber, N.,
692 Gutekunst, S., Harris, I., Haverd, V., Houghton, R. A., Hurtt, G., Ilyina, T., Jain, A.
693 K., Joetzjer, E., Kaplan, J. O., Kato, E., Goldewijk, K. K., Korsbakken, J. I.,
694 Landschuetzer, P., Lauvset, S. K., Lefevre, N., Lenton, A., Lienert, S., Lombardozzi,
695 D., Marland, G., McGuire, P. C., Melton, J. R., Metzl, N., Munro, D. R., Nabel, J. E.
696 M. S., Nakaoka, S.-I., Neill, C., Omar, A. M., Ono, T., Pregon, A., Pierrot, D.,
697 Poulter, B., Rehder, G., Resplandy, L., Robertson, E., Rodenbeck, C., Seferian, R.,
698 Schwinger, J., Smith, N., Tans, P. P., Tian, H., Tilbrook, B., Tubiello, F. N., van der
699 Werf, G. R., Wiltshire, A. J., and Zaehle, S.: Global Carbon Budget 2019, *Earth
700 System Science Data*, 11, 1783-1838, 10.5194/essd-11-1783-2019, 2019.

701 Friedrich, T., and Oschlies, A.: Neural network-based estimates of North Atlantic
702 surface $p\text{CO}_2$ from satellite data: A methodological study, *Journal of Geophysical
703 Research-Oceans*, 114, Artn C03020, 10.1029/2007jc004646, 2009.

704 Garcia, H., Weathers, K., Paver, C., Smolyar, I., Boyer, T., Locarnini, M., Zweng, M.,
705 Mishonov, A., Baranova, O., and Seidov, D.: World Ocean Atlas 2018. Vol. 4:
706 Dissolved Inorganic Nutrients (phosphate, nitrate and nitrate+ nitrite, silicate), 2019a.

707 Garcia, H., Weathers, K., Paver, C., Smolyar, I., Boyer, T., Locarnini, M., Zweng, M.,
708 Mishonov, A., Baranova, O., and Seidov, D.: World Ocean Atlas 2018, Volume 3:
709 Dissolved Oxygen, Apparent Oxygen Utilization, and Dissolved Oxygen Saturation,
710 2019b.

711 GLOBALVIEW-CO2: Cooperative Atmospheric Data Integration Project - Carbon
712 Dioxide [CD-ROM]. NOAA ESRL, B., Colo. (Ed.), [Available at ftp.cmdl.noaa.gov,
713 path: ccg/co2/GLOBALVIEW, 5th January 2013.], 2011.

714 González-Dávila, M., and Santana-Casiano, J.: Sea surface and atmospheric $f\text{CO}_2$ data
715 measured during the estoc time series cruises from 1995-2009, CDIAC, Oak Ridge
716 National Laboratory, US Department of Energy, Oak Ridge, Tennessee. doi, 10, 2009.

717 ~~Gregor, L., Lebehot, A. D., Kok, S., & Scheel Monteiro, P. M. A comparative~~
718 ~~assessment of the uncertainties of global surface ocean CO_2 estimates using a~~
719 ~~machine-learning ensemble (CSIR-ML6 version 2019a)–have we hit the wall?.~~
720 ~~Geoscientific Model Development, 12(12), 5113-5136, 2019.~~

721 Hales, B., Strutton, P. G., Saraceno, M., Letelier, R., Takahashi, T., Feely, R., Sabine,
722 C., and Chavez, F.: Satellite-based prediction of $p\text{CO}_2$ in coastal waters of the eastern
723 North Pacific, Prog Oceanogr, 103, 1-15, 10.1016/j.pocean.2012.03.001, 2012.

724 ~~Hu, C., Lee, Z., and Franz, B.: Chlorophyll a algorithms for oligotrophic oceans: A~~
725 ~~novel approach based on three-band reflectance difference, Journal of Geophysical~~
726 ~~Research: Oceans, 117, 10.1029/2011jc007395, 2012.~~

727 Huang, B., Thorne, P. W., Banzon, V. F., Boyer, T., Chepurin, G., Lawrimore, J. H.,
728 Menne, M. J., Smith, T. M., Vose, R. S., and Zhang, H.-M.: Extended reconstructed
729 sea surface temperature, version 5 (ERSSTv5): upgrades, validations, and
730 intercomparisons, J Climate, 30, 8179-8205, 2017.

731 ~~Iida, Y., Kojima, A., Takatani, Y., Nakano, T., Midorikawa, T., and Ishii, M.: Trends in~~
732 ~~$p\text{CO}_2$ and sea-air CO_2 flux over the global open oceans for the last two decades, J.~~
733 ~~Oceanogr., 71, 637–661, 10.1007/s10872-015-0306-4, 2015.~~

734 ~~Ishii, M., Feely, R. A., Rodgers, K. B., Park, G. H., Wanninkhof, R., Sasano, D.,~~
735 ~~Sugimoto, H., Cosea, C. E., Nakaoka, S., Telszewski, M., Nojiri, Y., Fletcher, S. E.~~
736 ~~M., Niwa, Y., Patra, P. K., Valsala, V., Nakano, H., Lima, I., Doney, S. C., Buitenhuis,~~
737 ~~E. T., Aumont, O., Dunne, J. P., Lenton, A., and Takahashi, T.: Air-sea CO_2 flux in~~
738 ~~the Pacific Ocean for the period 1990-2009, Biogeosciences, 11, 709-734,~~
739 ~~10.5194/bg-11-709-2014, 2014.~~

740 Jo, Y. H., Dai, M. H., Zhai, W. D., Yan, X. H., and Shang, S. L.: On the variations of
741 sea surface $p\text{CO}_2$ in the northern South China Sea: A remote sensing based neural
742 network approach, Journal of Geophysical Research-Oceans, 117, Artn C08022,
743 10.1029/2011jc007745, 2012.

744 ~~Keppler, L., and Landschützer, P.: Regional Wind Variability Modulates the Southern~~
745 ~~Ocean Carbon Sink, Scientific Reports, 9, ARTN 7384, 10.1038/s41598-019-43826-~~
746 ~~y, 2019.~~

747 Körtzinger, A.: Determination of carbon dioxide partial pressure ($p\text{CO}_2$), 3rd ed.,
748 Methods of Seawater Analysis, 3rd edn., 1999.

749 Landsch~~ü~~etzer, P., Gruber, N., Bakker, D. C. E., and Schuster, U.: Recent variability
750 of the global ocean carbon sink, *Glob. Biogeochem. Cycle*, 28, 927-949,
751 10.1002/2014gb004853, 2014.

752 Landsch~~ü~~etzer, P., Gruber, N., Bakker, D. C. E., Schuster, U., Nakaoka, S., Payne, M.
753 R., Sasse, T. P., and Zeng, J.: A neural network-based estimate of the seasonal to inter-
754 annual variability of the Atlantic Ocean carbon sink, *Biogeosciences*, 10, 7793-7815,
755 10.5194/bg-10-7793-2013, 2013.

~~756 Landsch~~ü~~etzer, P., Gruber, N., Haumann, A., Rodenbeck, C., Bakker, D. C. E., van
757 Heuven, S., Hoppema, M., Metzl, N., Sweeney, C., Takahashi, T., Tilbrook, B., and
758 Wanninkhof, R.: The reinvigoration of the Southern Ocean carbon sink, *Science*, 349,
759 1221-1224, 10.1126/science.aab2620, 2015.~~

760 Landsch~~ü~~etzer, P., Gruber, N., and Bakker, D. C. E.: Decadal variations and trends of
761 the global ocean carbon sink, *Glob. Biogeochem. Cycle*, 30, 1396-1417,
762 10.1002/2015gb005359, 2016.

763 Landsch~~ü~~etzer, P., Laruelle, G. G., Roobaert, A., and Regnier, P.: A uniform $p\text{CO}_2$
764 climatology combining open and coastal oceans, *Earth Syst. Sci. Data Discuss.*, 2020,
765 1-30, 10.5194/essd-2020-90, 2020.

766 Laruelle, G. G., Landsch~~ü~~etzer, P., Gruber, N., Tison, J. L., Delille, B., and Regnier, P.:
767 Global high-resolution monthly $p\text{CO}_2$ climatology for the coastal ocean derived from
768 neural network interpolation, *Biogeosciences*, 14, 4545-4561, 10.5194/bg-14-4545-
769 2017, 2017.

770 Marrec, P., Cariou, T., Mace, E., Morin, P., Salt, L. A., Vernet, M., Taylor, B., Paxman,
771 K., and Bozec, Y.: Dynamics of air-sea CO_2 fluxes in the northwestern European
772 shelf based on voluntary observing ship and satellite observations, *Biogeosciences*,
773 12, 5371-5391, 10.5194/bg-12-5371-2015, 2015.

774 Marshall G J.: Trends in the Southern Annular Mode from observations and reanalyses,
775 *Journal of climate*, 16, 10.1175/1520-0442(2003)016<4134:TITSAM>2.0.CO;2,
776 4134-4143, 2003.

777 Menemenlis, D., Campin, J.-M., Heimbach, P., Hill, C., Lee, T., Nguyen, A., Schodlok,
778 M., and Zhang, H.: ECCO2: High Resolution Global Ocean and Sea Ice Data
779 Synthesis, *Mercator Ocean Quarterly Newsletter*, 2008.

780 Moussa, H., Benallal, M. A., Goyet, C., and Lefevre, N.: Satellite-derived CO_2 fugacity
781 in surface seawater of the tropical Atlantic Ocean using a feedforward neural network,
782 *Int J Remote Sens*, 37, 580-598, 10.1080/01431161.2015.1131872, 2016.

783 Nakaoka, S., Telszewski, M., Nojiri, Y., Yasunaka, S., Miyazaki, C., Mukai, H., and
784 Usui, N.: Estimating temporal and spatial variation of ocean surface $p\text{CO}_2$ in the
785 North Pacific using a self-organizing map neural network technique, *Biogeosciences*,
786 10, 6093-6106, 10.5194/bg-10-6093-2013, 2013.

~~787 [NASA Goddard Space Flight Center, Ocean Ecology Laboratory, Ocean Biology
788 Processing Group. Moderate-resolution Imaging Spectroradiometer \(MODIS\) Aqua
789 Chlorophyll Data; 2018 Reprocessing. NASA OB.DAAC, Greenbelt, MD, USA.
790 10.5067/AQUA/MODIS/L3M/CHL/2018, 2018.](#)~~

~~791 Regnier, P., Friedlingstein, P., Ciais, P., Mackenzie, F. T., Gruber, N., Janssens, I. A.,
792 Laruelle, G. G., Lauerwald, R., Luyssaert, S., Andersson, A. J., Arndt, S., Arnosti, C.,~~

793 ~~Borges, A. V., Dale, A. W., Gallego-Sala, A., Godderis, Y., Goossens, N., Hartmann,~~
794 ~~J., Heinze, C., Ilyina, T., Joos, F., LaRowe, D. E., Leifeld, J., Meysman, F. J. R.,~~
795 ~~Munhoven, G., Raymond, P. A., Spahni, R., Suntharalingam, P., and Thullner, M.:~~
796 ~~Anthropogenic perturbation of the carbon fluxes from land to ocean, *Nature*~~
797 ~~*Geoscience*, 6, 597-607, 10.1038/Ngeo1830, 2013.~~

798 Rödenbeck, C., Bakker, D. C. E., Metzl, N., Olsen, A., Sabine, C., Cassar, N., Reum,
799 F., Keeling, R. F., and Heimann, M.: Interannual sea-air CO₂ flux variability from an
800 observation-driven ocean mixed-layer scheme, *Biogeosciences*, 11, 4599-4613,
801 10.5194/bg-11-4599-2014, 2014.

802 Sabine, C. L., Feely, R. A., Gruber, N., Key, R. M., Lee, K., Bullister, J. L., Wanninkhof,
803 R., Wong, C. S., Wallace, D. W. R., Tilbrook, B., Millero, F. J., Peng, T. H., Kozyr,
804 A., Ono, T., and Rios, A. F.: The oceanic sink for anthropogenic CO₂, *Science*, 305,
805 367-371, DOI 10.1126/science.1097403, 2004.

806 ~~Sarma, V. V. S. S.: Monthly variability in surface pCO₂ and net air-sea CO₂ flux in the~~
807 ~~Arabian Sea, *Journal of Geophysical Research-Oceans*, 108, Artn 3255,~~
808 ~~10.1029/2001je001062, 2003.~~

809 Sarma, V. V. S. S., Saino, T., Sasaoka, K., Nojiri, Y., Ono, T., Ishii, M., Inoue, H. Y., and
810 Matsumoto, K.: Basin-scale pCO₂ distribution using satellite sea surface temperature,
811 Chl-a, and climatological salinity in the North Pacific in spring and summer, *Glob.*
812 *Biogeochem. Cycle*, 20, Artn Gb3005, 10.1029/2005gb002594, 2006.

813 ~~Schuster, U., McKinley, G. A., Bates, N., Chevallier, F., Doney, S. C., Fay, A. R.,~~
814 ~~Gonzalez-Davila, M., Gruber, N., Jones, S., Krijnen, J., Landschuetzer, P., Lefevre,~~
815 ~~N., Manizza, M., Mathis, J., Metzl, N., Olsen, A., Rios, A. F., Roedenbeck, C.,~~
816 ~~Santana-Casiano, J. M., Takahashi, T., Wanninkhof, R., and Watson, A. J.: An~~
817 ~~assessment of the Atlantic and Arctic sea-air CO₂ fluxes, 1990-2009, *Biogeosciences*,~~
818 ~~10, 607-627, 10.5194/bg-10-607-2013, 2013.~~

819 Shadwick, E. H., Thomas, H., Comeau, A., Craig, S. E., Hunt, C. W., and Salisbury, J.
820 E.: Air-Sea CO₂ fluxes on the Scotian Shelf: seasonal to multi-annual variability,
821 *Biogeosciences*, 7, 3851-3867, 10.5194/bg-7-3851-2010, 2010.

822 Signorini, S. R., Mannino, A., Najjar, R. G., Friedrichs, M. A. M., Cai, W. J., Salisbury,
823 J., Wang, Z. A., Thomas, H., and Shadwick, E.: Surface ocean pCO₂ seasonality and
824 sea-air CO₂ flux estimates for the North American east coast, *Journal of Geophysical*
825 *Research-Oceans*, 118, 5439-5460, 10.1002/jgrc.20369, 2013.

826 Takahashi, T., Sutherland, S. C., Feely, R. A., and Wanninkhof, R.: Decadal change of
827 the surface water pCO₂ in the North Pacific: A synthesis of 35 years of observations,
828 *Journal of Geophysical Research-Oceans*, 111, Artn C07s05, 10.1029/2005jc003074,
829 2006.

830 Takahashi, T., Sutherland, S. C., Wanninkhof, R., Sweeney, C., Feely, R. A., Chipman,
831 D. W., Hales, B., Friederich, G., Chavez, F., Sabine, C., Watson, A., Bakker, D. C. E.,
832 Schuster, U., Metzl, N., Yoshikawa-Inoue, H., Ishii, M., Midorikawa, T., Nojiri, Y.,
833 Kortzinger, A., Steinhoff, T., Hoppema, M., Olafsson, J., Arnarson, T. S., Tilbrook,
834 B., Johannessen, T., Olsen, A., Bellerby, R., Wong, C. S., Delille, B., Bates, N. R.,
835 and de Baar, H. J. W.: Climatological mean and decadal change in surface ocean

836 *p*CO₂, and net sea-air CO₂ flux over the global oceans, *Deep-Sea Research Part II-*
837 *Topical Studies in Oceanography*, 56, 554-577, 10.1016/j.dsr2.2008.12.009, 2009.

838 Telszewski, M., Chazottes, A., Schuster, U., Watson, A. J., Moulin, C., Bakker, D. C.
839 E., Gonzalez-Davila, M., Johannessen, T., Kortzinger, A., Luger, H., Olsen, A., Omar,
840 A., Padin, X. A., Rios, A. F., Steinhoff, T., Santana-Casiano, M., Wallace, D. W. R.,
841 and Wanninkhof, R.: Estimating the monthly *p*CO₂ distribution in the North Atlantic
842 using a self-organizing neural network, *Biogeosciences*, 6, 1405-1421, DOI
843 10.5194/bg-6-1405-2009, 2009.

844 Wang, Y., Li, X., Song, J., Zhong, G., and Zhang, B.: Carbon Sinks and Variations of
845 *p*CO₂ in the Southern Ocean from 1998 to 2018 Based on a Deep Learning Approach,
846 *IEEE Journal of Selected Topics in Applied Earth Observations and Remote Sensing*,
847 2021.

848 ~~Wanninkhof, R., Park, G. H., Takahashi, T., Sweeney, C., Feely, R., Nojiri, Y., Gruber,~~
849 ~~N., Doney, S. C., McKinley, G. A., Lenton, A., Le Quere, C., Heinze, C., Schwinger,~~
850 ~~J., Graven, H., and Khatiwala, S.: Global ocean carbon uptake: magnitude, variability~~
851 ~~and trends, *Biogeosciences*, 10, 1983-2000, 10.5194/bg-10-1983-2013, 2013.~~

852 Watson, A. J., Schuster, U., Shutler, J. D., Holding, T., Ashton, I. G. C., Landschützer,
853 P., Woolf, D. K., and Goddijn-Murphy, L.: Revised estimates of ocean-atmosphere
854 CO₂ flux are consistent with ocean carbon inventory, *Nature Communications*, 11,
855 10.1038/s41467-020-18203-3, 2020.

856 Weiss, R. F.: Carbon dioxide in water and seawater: the solubility of a non-ideal gas,
857 *Marine Chemistry*, 2, 203--215, 1974.

858 Zeng, J., Nojiri, Y., Landschützer, P., Telszewski, M., and Nakaoka, S.: A Global
859 Surface Ocean *f*CO₂ Climatology Based on a Feed-Forward Neural Network, *Journal*
860 *of Atmospheric and Oceanic Technology*, 31, 1838-1849, 10.1175/jtech-d-13-
861 00137.1, 2014.

862 Zeng, J. Y., Nojiri, Y., Nakaoka, S., Nakajima, H., and Shirai, T.: Surface ocean CO₂ in
863 1990-2011 modelled using a feed-forward neural network, *Geosci Data J*, 2, 47-51,
864 10.1002/gdj3.26, 2015.

865 Zeng, J. Y., Matsunaga, T., Saigusa, N., Shirai, T., Nakaoka, S., and Tan, Z. H.:
866 Technical note: Evaluation of three machine learning models for surface ocean CO₂
867 mapping, *Ocean Sci*, 13, 303-313, 10.5194/os-13-303-2017, 2017.

868 Zhong, G., Li, X., Qu, B., Wang, Y., Yuan, H., and Song, J.: A General Regression Neural
869 Network approach to reconstruct global 1°×1° resolution sea surface *p*CO₂, *Acta*
870 *Oceanol Sin*, 10, 70-79, 10.3969/j.issn.0253-4193.2020.10.007, 2020.